Nanoscale Protein Patterning via Nanoimprint Lithography and Ultrafast Laser Irradiation

by

Jeremy Damon Hoff

A dissertation submitted in partial fulfillment
of the requirements for the degree of
Doctor of Philosophy
(Biomedical Engineering)
in The University of Michigan
2009

Doctoral Committee:

Associate Professor Alan J Hunt, Chair
Professor Edgar Meyhofer
Professor Steven M Yalisove
Associate Professor L Jay Guo
Associate Professor Shuichi Takayama

To my Family

ACKNOWLEDGEMENTS

A project of this length and scope invariably involves contributions from many individuals and organizations, whether in the form of material, intellectual, or emotional support. I am grateful for the helpful contributions of all who have aided me over the past several years, with special thanks to the following.

I would especially like to thank Alan Hunt and Edgar Meyhofer for their support, guidance in the pursuit of a scientific career, and for their ability and willingness to ask tough questions when warranted.

I would like to extend gratitude for the support, thoughtful conversations, and friendship provided by all the members of the Hunt lab: Henry Schek, David Lorch, Blake Charlebois Kevin Ke, Elissa Burk, Jeffrey Herbstman, Ran An, Jun Chung, and Gary Brouhard.

Of course, none of this work would be possible without generous financial support. During the course of my studies, my work has been funded, directly or indirectly, by DARPA, NIH, NSF, the University of Michigan Institute of Gerontology, and the Burroughs Wellcome Fund.

TABLE OF CONTENTS

LIST OF FIGURES

CHAPTER 1

INTRODUCTION

The biological functions of proteins are extraordinarily diverse and include catalysis, force generation, mechanical support, signaling and sensing. The immobilization of proteins on surfaces to take advantage of this biological functionality has a long history in biotechnology, enabling a wide variety of biological assays and biotechnological applications to take advantage of proteins' diverse range of functionalities. Protein-coated surfaces are used to purify proteins in affinity chromatography, detect biomolecules via their interaction with immobilized antibodies or receptors, and functionalize surfaces to aid cellular growth, to name but a few applications[1]. Proteins immobilized uniformly and/or randomly on surfaces enable these and many other applications. Confining the placement of proteins to designated regions while excluding them from other regions, though, greatly extends the potential applications of protein immobilization. This selective placement of proteins, protein patterning, allows the segregation of protein functionalities in spatially separated regions of a substrate. Incorporating many different functionalities in a single device or assay, with precise control over the spatial arrangement of each protein function, significantly enhances the usefulness of protein immobilization, enabling

development of a wide variety of micro- or nano-scale devices and applications, including biosensors, integrated bioMEMS, and basic biological assays.

For example, patterning an array of many different antibodies on a proteomic chip allows the simultaneous detection of a large number of different potential biomarkers. Screening against many targets at once facilitates the discovery of new biomarkers for diseases or other conditions[2]. It is also useful in developing a more complete "biosignature" of a particular disease or patient[3;4]. These functions allow for better diagnosis, characterization, and treatment of disease, and potentially facilitate individualized treatments based on a patient's protein expression profile.

Patterned proteins also enable development of integrated bioMEMS, making use of proteins to perform sensing, transport, or actuating functions in an integrated microdevice. For instance, Lin et al demonstrated a biomolecularly powered sorting and concentrating device in which tubelike biological polymers, microtubules, bind a target analyte and are propelled by the motor protein kinesin to accumulate in a concentration chamber[5], and a number of other groups have used motor proteins such as kinesin or myosin to similarly transport molecular cargo or generate forces in biochemically powered actuators in microdevices[6-13].

Fine control of the placement of proteins also enables or facilitates a wide variety of basic biological assays in which the geometric spacing or distribution is of import. For example, the growth and activity of cells are influenced heavily by the distribution of extracellular signaling molecules it encounters. To describe one particular example, the formation of focal contacts, which plays a critical role in cell cycle regulation, influencing cell migration, proliferation, and apoptosis[14], involves the clustering of the cell adhesion receptor protein integrin. Protein patterning techniques have allowed several groups to observe that a cell will more readily form focal contacts when encountering integrin ligands, such as fibronectin, arranged in clusters, as opposed to encountering an equivalent average surface density of ligand distributed uniformly[15-17] A number of other recent studies have used micro- or nano-scale protein patterning to probe the importance of the spatial arrangement of extracellular signal molecules on cellular behaviors, including cell morphology and adhesion[18], dendritic branching[19], cell migration[20], cell cycle regulation[21;22] and mechanotransduction[23], and immunologic response[24;25].

1.1 Protein Patterning Goals:

Most protein patterning techniques share three basic aims:

1) **High specificity or contrast**: It is generally desirable to achieve a high density of target proteins in the designated regions while minimizing their

adsorption in other regions. This improves, for instance, the signal to noise ratio of an antibody-based biosensor, and thus its sensitivity and speed. In practice, generating dense protein coverage in the designated regions is relatively simple. A wide variety of surface functionalizations are commonly used to bind proteins to substrates[26]. Proteins will generally, in fact, bind non-specifically to most surfaces (see [27] for a thorough discussion of the factors influencing non-specific protein adsorption). There-in lies a primary challenge for protein patterning methods: preventing the adsorption of target proteins in undesignated regions. Devices exposed to biological media are inevitably fouled with proteins, progessively corrupting their ability to perform their desired function The most common methods used to minimize such undesirable adsorption usually involve the use of relatively high concentrations of blocking proteins such as BSA or casein which dominate non-specific binding while the relatively sparse target protein binds via a specific binding interaction[28], the use of polyethylene glycol-coated surfaces, whose compression by protein binding is entropically unfavorable[29;30], or restricting the dispensation of protein-containing solution to designated areas[31;32].

2) **High resolution:** Minimizing the size of patterned features has a number of advantages. Biosensor applications, for example, can be expected to be more sensitive[2] and produce faster results while requiring less

analyte and reagents with small, high-density patterns of sensing proteins[33]. Additionally, increasing the resolution enables proteins to be immobilized in more physiologically relevant geometries. As noted above, the nanoscale spatial arrangement of signal proteins significantly influences a variety of cellular activities. At the extreme, resolutions near 10nm may enable the directed placement of individual proteins, facilitating single molecule assays.

3) **Maintain bioactivity:** It is essential that patterned proteins retain at least some of their native biological function, whether the function is mechanical, sensing, signaling, or catalytic. The protein must be properly oriented on the substrate so as to maintain this activity. This generally means that the protein must be immobilized such that the active site is oriented away from the substrate and is available for interaction with reactants or binding partners[34]. The denaturation, or misfolding, of the protein must also be minimized in order to affect minimal disruption in the proteins' functions[26]. Though conformational change is inevitable as the protein interacts with an interface[34;35], considerable attention has been given to minimizing the deleterious effects of various immobilization strategies on the activity of immobilized proteins[36-40].

1.2 Overview of existing patterning techniques

A variety of techniques have been developed to pattern proteins on planar substrates. These techniques have been reviewed in detail elsewhere[41;42], but we will introduce some of the more common methods.

Photolithography

For decades, the semiconductor industry has used and optimized photolithographic methods to generate high resolution features in semiconductors and metals. In photolithography, a substrate is coated with a photoactive polymer. When portions of this polymer are selectively exposed to light, the solubility of the exposed regions is altered, such that the exposed regions can be selectively dissolved while leaving the unexposed regions unaffected (or vice versa, depending on the photoactive polymer chosen). This development step leaves portions of the underlying substrate exposed for further modification, such as etching, doping, or metal coating.

More recently, these methods have been applied to generating protein patterns. A number of particular implementations have been demonstrated, but in general the substrate regions exposed after development are functionalized so as to bind, or promote binding of, target proteins. For example, an exposed silicon

dioxide surface may be covalently modified with an aminosilane, leaving a reactive amine group which can preferentially bind proteins[43;44].

Photolithography is a mature technology, optimized over many years by the semiconductor industry, and this extensive development makes it an attractive technique for microscale protein patterning. The resolution of these techniques is fundamentally limited, though, by the diffraction limit of the light used during exposure. Additionally, the harsh chemicals typically used limit the compatibility of the process with biological media, though progress has been made in the development of biocompatible photoresists[45]

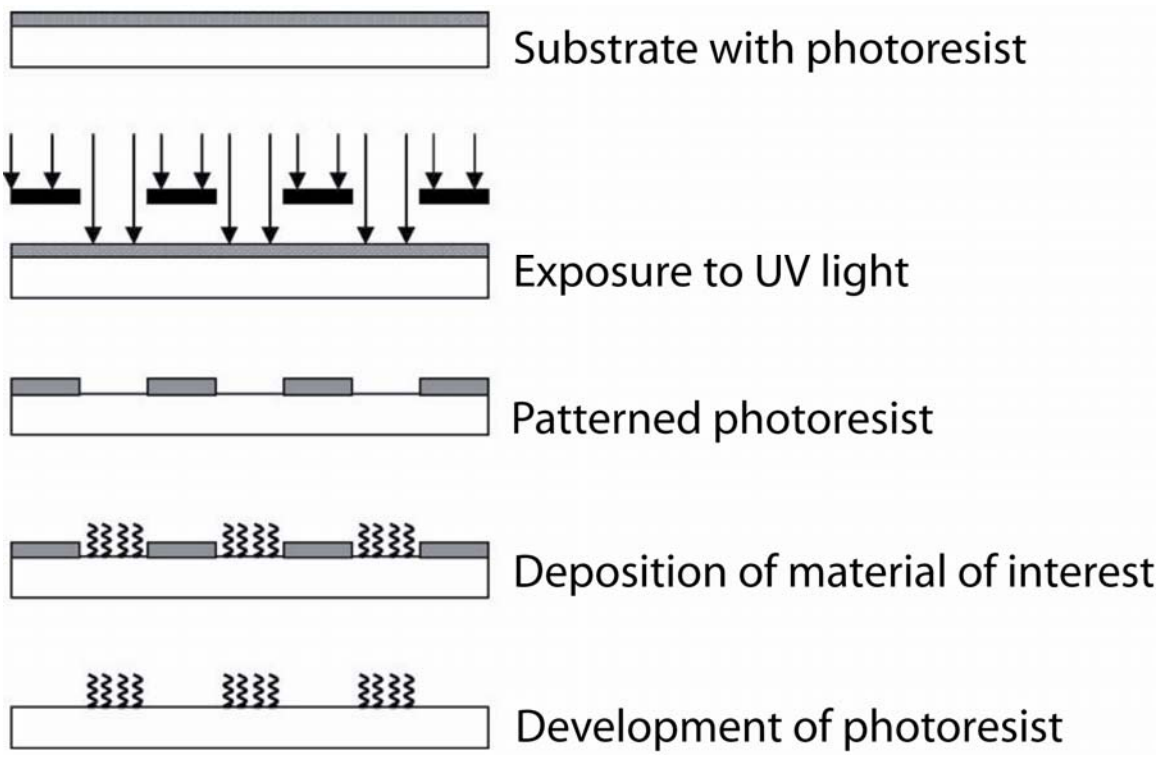

Figure 1-1: Protein patterning using photolithography. A photoactive polymer is selectively exposed to light, exposing regions of the underlying substrate. The substrate is then functionalized with a molecule such as an aminosilane which promotes protein binding. Image from ref. [46]

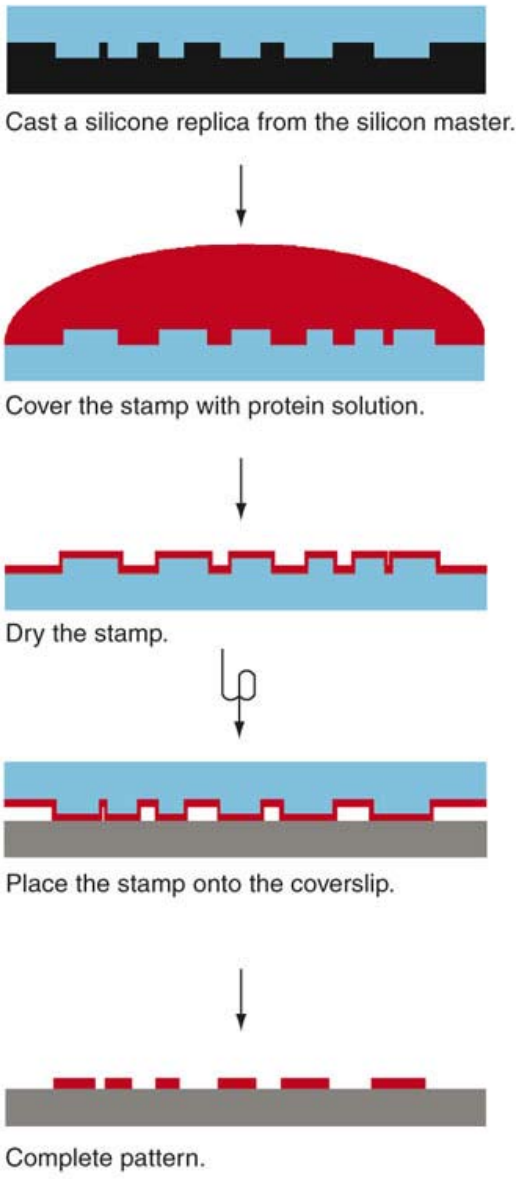

Figure 1-2: Protein patterning by microcontact printing. A polymeric stamp is molded from a solid master. The stamp is coated with protein-containing solution and allowed to dry. The stamp is them brought into contact with the substrate to be patterned, transferring the target protein to the substrate. Image from ref. [47]

Microcontact Printing

The patterning technique of microcontact printing resembles rubber-stamping of ink. In this technique, a polymeric mold is fabricated from a template. A drop of

protein solution “ink” is deposited on the mold, and the mold is brought into gentle contact with the substrate to be modified. The protein solution is transferred from the protrusions in the mold to the substrate. The use of a broadly biologically friendly polymer, PDMS, for the mold material makes this technique highly biocompatible[48-50]. Depending primarily on the technique used to fabricate the initial template from which the mold is generated, this technique is capable of features from hundreds of microns down to tens of nanometers[51]. Some disadvantages of this technique lie in the potential of the flexible polymeric mold to generate deformed or distorted patterns, non-uniformity of coverage over the patterned area, and potential for surface contamination of the stamp[52]..

Dip-pen nanolithography

Patterning via dip-pen nanolithography is similar conceptually to writing using a quill and ink. An AFM tip is dipped in an “ink” solution containing protein or a cross-linking molecule which will bind protein in subsequent steps. The coated tip is then dragged across the substrate, leaving a trail of target molecule in the vicinity of its path. This technique is capable of very small feature sizes, down to tens of nanometers[53], and can conceivably place an arbitrary number of different protein types by using different ink solutions[54]. However, due to its serial nature and the limited amount of “ink” that can be loaded on each loaded tip, this technique is slow and cannot easily generate large patterns.

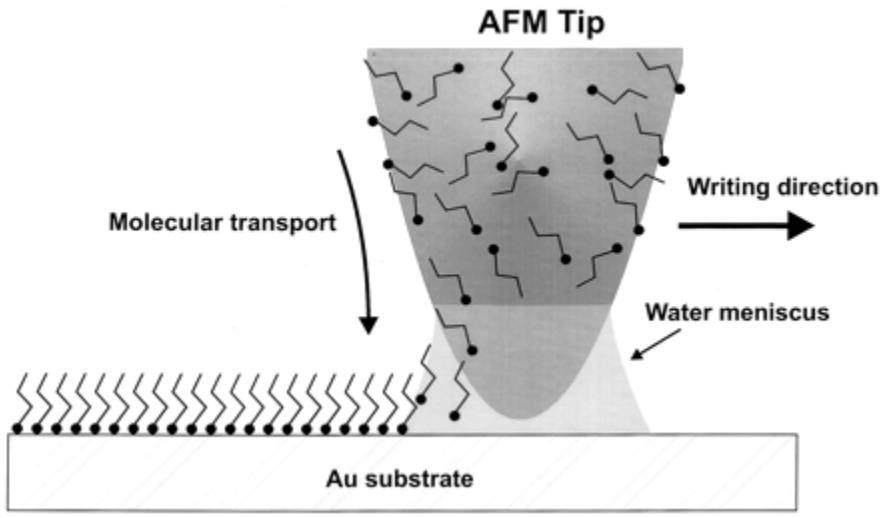

Figure 1-3: Biomolecule patterning using dip-pen nanolithography. An AFM tip is coated with a biomolecule of interest and scanned across the substrate to be patterned, transferring molecules to the substrate as it moves. In this image, amine-thiol groups are being transferred to a gold substrate which can be subsequently modified with proteins or other biomolecules. Image from ref. [53]

Ink-jet printing

So-called ink-jet printing of proteins makes use of a mechanism very similar to what one would find in a desktop ink-jet printer. Protein-containing solution is loaded into a channel. Pressure is applied on the fluid in the channel, for example by expansion of a piezoelectric wall or rapid localized heating, causing a droplet of solution to be expelled onto a substrate[55-58].

This technique is relatively inexpensive, simple, and based on existing commercial technology. By placing the protein solution only in designated regions, the technique avoids problems associated with non-specific binding of target proteins outside of the desired region. Its primary disadvantage is that the feature size is generally limited to tens of microns[55].

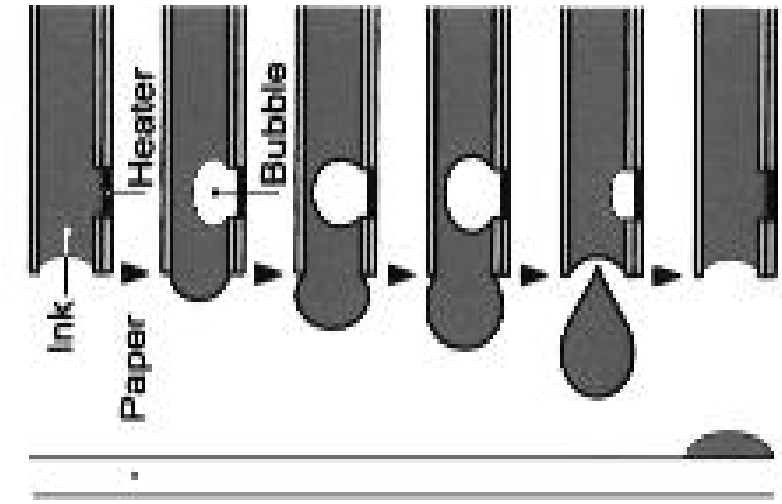

Figure 1-4: Ink-jet printing of proteins. A protein-containing solution is loaded into a chamber. Pressure is applied to the fluid, by thermally generating a bubble in this case, causing a droplet of solution to be expelled onto the underlying substrate. Image from ref. [32]

Self-assembled patterns

A number variety of techniques have demonstrated that under certain conditions, molecules may self-assemble into distinct geometries. These shapes can be functionalized, generating protein patterns which follow the self-assembled geometries, or act as a mask for functionalization of the underlying substrate.

For example, some groups have used micro- or nano-scale spheres which self-assemble into a close-packed pattern on a surface to create a colloidal mask. Biomolecules can be adsorbed in the interstices between the spheres, leaving a hexagonal pattern of the target biomolecule on the surface after the spheres are removed. Protein feature sizes down to tens of nanometers have been demonstrated with this technique. [59;60].

Other groups have used lattices of DNA tiles to create protein arrays. The sticky ends of the DNA tiles are engineered to self-assemble into a regular array. Periodic patterns of the protein streptavidin were demonstrated by Yan et al. by incorporating a biotin group in the center of each tile, giving a regular spacing between individual streptavidin molecules of approximately 19nm[61]. By engineering multiple tiles which self-assemble into more complicated geometries, and incorporating biotin into only a portion of them, the spacing between streptavidin molecules can be modified[62].

Bacterial membrane support proteins, S-layers, self-assemble into periodic lattices of various geometries, and have also been functionalized to serve as a scaffold to generate regular periodic patterns of biomolecules such as streptavidin, with individual proteins arrayed with approximately 10nm spacing[63].

Broadly, these self-assembly techniques are capable of generating periodic patterns with extremely small feature sizes over wide areas. However, variation and control of the resultant geometries is limited. The feature size and spacing over the entire patterned region are predetermined by the choice of templating molecules or particles.

1.3 Chapter Summary

We have sought to expand the protein patterning toolset available to biologists and bioengineers by developing two broad approaches capable of producing high resolution patterns of protein with high specificity. In Chapter 2, we describe the use of nano-imprint lithography (NIL) with subsequent modification with a passivating surface chemical modification to generate sub-100nm protein feature sizes. NIL offers the advantages of high-throughput, low-cost, and high-reproducibility; and the capability of creating nanopatterns with features as small as 10 nm over large areas

The second high resolution patterning technique developed, described in Chapter 3, involves the selective removal of protein from glass surfaces using tightly focused ultrafast laser irradiation. Due to the highly non-linear damage mechanism, ultrafast laser irradiation is well-known to be capable of ablating material volumes much smaller than the focal volume of the laser. We first review the mechanisms behind this phenomenon, and also discusses potential damage mechanisms involved in material damage below the critical ablation threshold for glass, where obvious catastrophic material damage (e.g. ablation) is not observed. The latter discussion is particularly pertinent, as the protein removal we demonstrate results from single pulses of intensity significantly below the ablation threshold. This allows cleaning of the surface without damaging the underlying substrate. AFM and epifluorescent analyses indicate near-total

removal of proteins from the glass surface with well-defined nanoscale features. We describe potential mechanisms for the damage and/or removal of proteins from the surface based on the photolytic generation of free electrons.

Chapter 4 further probes the interaction of sub-threshold laser irradiation at the glass-biological media interface. We characterize the adsorption of several model proteins as well as small charged fluorophores on irradiated glass surfaces. We also observe the effect on the adsorptivity of protein-coated surfaces exposed to ultrafast irradiation. Based on the adsorptive behaviors of the proteins or fluorophores in these studies, we describe a sub-threshold damage mechanism which alters the long-term chemical state, surface charge, and adsorptivity of irradiated glass surfaces.

In addition to demonstrating a new high-resolution protein patterning technique, the mechanisms described in Chapters 3 and 4 lead to a better understanding of sub-threshold laser interactions with both glass and biological media. Understanding the mechanism behind interactions with biological media is important in interpreting the results of applications relying on damage to biological material with ultrafast pulses. Such biological applications of ultrafast laser-induced damage are diverse, including ocular surgery[64-66], membrane poration[67;68], single neuron axotomy in C. elegans[69], and intracellular dissection of individual chromosomes[70] or mitochondria[71]. Additionally, it is

important to consider unintended damage effects in applications such as ultrafast multiphoton microscopy and spectroscopy[72-74].

The discussion of the adsorption of proteins on irradiated glass, and the mechanism by which this adsorptive behavior is changed due to the irradiation, also contributes to an understanding of the influence of surface charge on the bioactivity of immobilized proteins. The behavior of immobilized proteins is heavily influenced by the mechanics of adsorption, which may effect the degree of denaturation and protein orientation, and thus their enzymatic activity and/or ability interact with desired partners[1;37;75]. This discussion thus has relevance to the bioactivity of immobilized proteins, a critical concern in any device or application requiring interaction with immobilized proteins.

Finally, in Chapter 5 we describe the guidance of motile fibroblasts by selectively removing the extracellular matrix protein fibronectin from the cells' path through use of the laser-based protein removal technique mentioned above. Control of cellular behavior by presenting the cell with a surface selectively coated with extracellular signal proteins such as fibronectin has been demonstrated by a variety of patterning techniques[15;76;77]. However, our method provides a general technique to modify the cellular microenvironment *in situ*, and thereby presents itself as a useful tool for study of cellular response to changes in extracellular environment imposed during observation. Though we demonstrate this on a 2-dimensional glass substrate, the technique is plausibly extensible to

modification of the 3-dimensional micro-environment. This extensibility would make it possible to study cells in a situation much closer to their native environment.

Reference List

[1] Lu,B., Smyth,M.R., OKennedy,R., Oriented immobilization of antibodies and its applications in immunoassays and immunosensors, Analyst, 121 (1996) R29-R32.

[2] Silzel,J.W., Cercek,B., Dodson,C., Tsay,T., Obremski,R.J., Mass-sensing, multianalyte microarray immunoassay with imaging detection, Clinical Chemistry, 44 (1998) 2036-2043.

[3] Wilson,D.S., Nock,S., Recent developments in protein microarray technology, Angewandte Chemie-International Edition, 42 (2003) 494-500.

[4] Walter,G., Bussow,K., Lueking,A., Glokler,J., High-throughput protein arrays: prospects for molecular diagnostics, Trends in Molecular Medicine, 8 (2002) 250-253.

[5] Lin,C.T., Kao,M.T., Kurabayashi,K., Meyhofer,E., Self-contained biomolecular motor-driven protein sorting and concentrating in an ultrasensitive microfluidic chip, Nano Letters, 8 (2008) 1041-1046.

[6] Hess,H., Bachand,G.D., Vogel,V., Powering nanodevices with biomolecular motors, Chemistry-A European Journal, 10 (2004) 2110-2116.

[7] Bachand,G.D., Rivera,S.B., Boal,A.K., Gaudioso,J., Liu,J., Bunker,B.C., Assembly and transport of nanocrystal CdSe quantum dot nanocomposites

using microtubules and kinesin motor proteins, Nano Letters, 4 (2004) 817-821.

[8] Hiratsuka,Y., Tada,T., Oiwa,K., Kanayama,T., Uyeda,T.Q.P., Controlling the direction of kinesin-driven microtubule movements along microlithographic tracks, Biophysical Journal, 81 (2001) 1555-1561.

[9] Moorjani,S.G., Jia,L., Jackson,T.N., Hancock,W.O., Lithographically patterned channels spatially segregate kinesin motor activity and effectively guide microtubule movements, Nano Letters, 3 (2003) 633-637.

[10] Jaber,J.A., Chase,P.B., Schlenoff,J.B., Actomyosin-driven motility on patterned polyelectrolyte mono- and multilayers, Nano Letters, 3 (2003) 1505-1509.

[11] Diez,S., Reuther,C., Dinu,C., Seidel,R., Mertig,M., Pompe,W., Howard,J., Stretching and transporting DNA molecules using motor proteins, Nano Letters, 3 (2003) 1251-1254.

[12] Spetzler,D., York,J., Dobbin,C., Martin,J., Ishmukhametov,R., Day,L., Yu,J., Kang,H., Porter,K., Hornung,T., Frasch,W.D., Recent developments of bio-molecular motors as on-chip devices using single molecule techniques, Lab on A Chip, 7 (2007) 1633-1643.

[13] Yokokawa,R., Takeuchi,S., Kon,T., Nishiura,M., Sutoh,K., Fujita,H., Unidirectional transport of kinesin-coated beads on microtubules oriented in a microfluidic device, Nano Letters, 4 (2004) 2265-2270.

[14] Bourdoulous,S., Orend,G., MacKenna,D.A., Pasqualini,R., Ruoslahti,E., Fibronectin matrix regulates activation of Rho and Cdc42 GTPases and cell cycle progression, Journal of Cell Biology, 143 (1998) 267-276.

[15] Chen,C.S., Mrksich,M., Huang,S., Whitesides,G.M., Ingber,D.E., Geometric control of cell life and death, Science, 276 (1997) 1425-1428.

[16] Arnold,M., Cavalcanti-Adam,E.A., Glass,R., Blummel,J., Eck,W., Kantlehner,M., Kessler,H., Spatz,J.P., Activation of integrin function by nanopatterned adhesive interfaces, Chemphyschem, 5 (2004) 383-388.

[17] Maheshwari,G., Brown,G., Lauffenburger,D.A., Wells,A., Griffith,L.G., Cell adhesion and motility depend on nanoscale RGD clustering, Journal of Cell Science, 113 (2000) 1677-1686.

[18] Lehnert,D., Wehrle-Haller,B., David,C., Weiland,U., Ballestrem,C., Imhof,B.A., Bastmeyer,M., Cell behaviour on micropatterned substrata: limits of extracellular matrix geometry for spreading and adhesion, Journal of Cell Science, 117 (2004) 41-52.

[19] Craighead,H.G., Turner,S.W., Davis,R.C., James,C., Perez,A.M., St.John,P.M., Isaacson,M.S., Kam,L., Shain,W., Turner,J.N., Banker,G., Chemical and Topographical Surface Modification for Control of Central Nervous System Cell Adhesion, Biomedical Microdevices, 1 (1998) 49-63.

[20] Jiang,X.Y., Bruzewicz,D.A., Wong,A.P., Piel,M., Whitesides,G.M., Directing cell migration with asymmetric micropatterns, Proceedings of the National Academy of Sciences of the United States of America, 102 (2005) 975-978.

[21] Dike,L.E., Chen,C.S., Mrksich,M., Tien,J., Whitesides,G.M., Ingber,D.E., Geometric control of switching between growth, apoptosis, and differentiation during angiogenesis using micropatterned substrates, In Vitro Cellular & Developmental Biology-Animal, 35 (1999) 441-448.

[22] Huang,S., Chen,C.S., Ingber,D.E., Control of cyclin D1, p27(Kip1), and cell cycle progression in human capillary endothelial cells by cell shape and cytoskeletal tension, Molecular Biology of the Cell, 9 (1998) 3179-3193.

[23] Chen,C.S., Tan,J., Tien,J., Mechanotransduction at cell-matrix and cell-cell contacts, Annual Review of Biomedical Engineering, 6 (2004) 275-302.

[24] Wu,M., Holowka,D., Craighead,H.G., Baird,B., Visualization of plasma membrane compartmentalization with patterned lipid bilayers, Proceedings of the National Academy of Sciences of the United States of America, 101 (2004) 13798-13803.

[25] Doh,J., Irvine,D.J., Immunological synapse arrays: Patterned protein surfaces that modulate immunological synapse structure formation in T cells, Proceedings of the National Academy of Sciences of the United States of America, 103 (2006) 5700-5705.

[26] Rusmini,F., Zhong,Z.Y., Feijen,J., Protein immobilization strategies for protein biochips, Biomacromolecules, 8 (2007) 1775-1789.

[27] Norde,W., Adsorption of Proteins from Solution at the Solid-Liquid Interface, Advances in Colloid and Interface Science, 25 (1986) 267-340.

[28] Vogt,R.F., Phillips,D.L., Henderson,L.O., Whitfield,W., Spierto,F.W., Quantitative Differences Among Various Proteins As Blocking-Agents for Elisa Microtiter Plates, Journal of Immunological Methods, 101 (1987) 43-50.

[29] Gombotz,W.R., Guanghui,W., Horbett,T.A., Hoffman,A.S., Protein Adsorption to Poly(Ethylene Oxide) Surfaces, Journal of Biomedical Materials Research, 25 (1991) 1547-1562.

[30] Bergstrom,K., Osterberg,E., Holmberg,K., Hoffman,A.S., Schuman,T.P., Kozlowski,A., Harris,J.M., Effects of Branching and Molecular-Weight of Surface-Bound Poly(Ethylene Oxide) on Protein Rejection, Journal of Biomaterials Science-Polymer Edition, 6 (1994) 123-132.

[31] Bruckbauer,A., Zhou,D.J., Kang,D.J., Korchev,Y.E., Abell,C., Klenerman,D., An addressable antibody nanoarray produced on a nanostructured surface, Journal of the American Chemical Society, 126 (2004) 6508-6509.

[32] Okamoto,T., Suzuki,T., Yamamoto,N., Microarray fabrication with covalent attachment of DNA using Bubble Jet technology, Nature Biotechnology, 18 (2000) 438-441.

[33] Wingren,C., Borrebaeck,C.A.K., Progress in miniaturization of protein arrays - a step closer to high-density nanoarrays, Drug Discovery Today, 12 (2007) 813-819.

[34] Andrade,J.D., Hlady,V., Protein Adsorption and Materials Biocompatibility - A Tutorial Review and Suggested Hypotheses, Advances in Polymer Science, 79 (1986) 1-63.

[35] Firestone,M.A., Shank,M.L., Sligar,S.G., Bohn,P.W., Film architecture in biomolecular assemblies. Effect of linker on the orientation of genetically engineered surface-bound proteins, Journal of the American Chemical Society, 118 (1996) 9033-9041.

[36] Spitznagel,T.M., Clark,D.S., Surface-Density and Orientation Effects on Immobilized Antibodies and Antibody Fragments, Bio-Technology, 11 (1993) 825-829.

[37] Chen,S.F., Liu,L.Y., Zhou,J., Jiang,S.Y., Controlling antibody orientation on charged self-assembled monolayers, Langmuir, 19 (2003) 2859-2864.

[38] Vijayendran,R.A., Leckband,D.E., A quantitative assessment of heterogeneity for surface-immobilized proteins, Analytical Chemistry, 73 (2001) 471-480.

[39] Peluso,P., Wilson,D.S., Do,D., Tran,H., Venkatasubbaiah,M., Quincy,D., Heidecker,B., Poindexter,K., Tolani,N., Phelan,M., Witte,K., Jung,L.S., Wagner,P., Nock,S., Optimizing antibody immobilization strategies for the

construction of protein microarrays, Analytical Biochemistry, 312 (2003) 113-124.

[40] Andrade,J.D., Hlady,V., Wei,A.P., Adsorption of Complex Proteins at Interfaces, Pure and Applied Chemistry, 64 (1992) 1777-1781.

[41] Christman,K.L., Enriquez-Rios,V.D., Maynard,H.D., Nanopatterning proteins and peptides, Soft Matter, 2 (2006) 928-939.

[42] Blawas,A.S., Reichert,W.M., Protein patterning, Biomaterials, 19 (1998) 595-609.

[43] Lom,B., Healy,K.E., Hockberger,P.E., A Versatile Technique for Patterning Biomolecules Onto Glass Coverslips, Journal of Neuroscience Methods, 50 (1993) 385-397.

[44] Britland,S., Perezarnaud,E., Clark,P., Mcginn,B., Connolly,P., Moores,G., Micropatterning Proteins and Synthetic Peptides on Solid Supports - A Novel Application for Microelectronics Fabrication Technology, Biotechnology Progress, 8 (1992) 155-160.

[45] Douvas,A., Argitis,P., Misiakos,K., Dimotikali,D., Petrou,P.S., Kakabakos,S.E., Biocompatible photolithographic process for the patterning of biomolecules, Biosensors & Bioelectronics, 17 (2002) 269-278.

[46] Yap,F.L., Zhang,Y., Protein and cell micropatterning and its integration with micro/nanoparticles assembly, Biosensors & Bioelectronics, 22 (2007) 775-788.

[47] Von Philipsborn,A.C., Lang,S., Bernard,A., Loeschinger,J., David,C., Lehnert,D., Bastmeyer,M., Bonhoeffer,F., Microcontact printing of axon guidance molecules for generation of graded patterns, Nature Protocols, 1 (2006) 1322-1328.

[48] Bernard,A., Delamarche,E., Schmid,H., Michel,B., Bosshard,H.R., Biebuyck,H., Printing patterns of proteins, Langmuir, 14 (1998) 2225-2229.

[49] Kane,R.S., Takayama,S., Ostuni,E., Ingber,D.E., Whitesides,G.M., Patterning proteins and cells using soft lithography, Biomaterials, 20 (1999) 2363-2376.

[50] Xia,Y.N., Whitesides,G.M., Soft lithography, Annual Review of Materials Science, 28 (1998) 153-184.

[51] Csucs,G., Kunzler,T., Feldman,K., Robin,F., Spencer,N.D., Microcontact printing of macromolecules with submicrometer resolution by means of polyolefin stamps, Langmuir, 19 (2003) 6104-6109.

[52] Torres,A.J., Wu,M., Holowka,D., Baird,B., Nanobiotechnology and cell biology: Micro- and nanofabricated surfaces to investigate receptor-mediated signaling, Annual Review of Biophysics, 37 (2008) 265-288.

[53] Piner,R.D., Zhu,J., Xu,F., Hong,S.H., Mirkin,C.A., "Dip-pen" nanolithography, Science, 283 (1999) 661-663.

[54] Hong,S.H., Zhu,J., Mirkin,C.A., Multiple ink nanolithography: Toward a multiple-pen nano-plotter, Science, 286 (1999) 523-525.

[55] Barron,J.A., Young,H.D., Dlott,D.D., Darfler,M.M., Krizman,D.B., Ringeisen,B.R., Printing of protein microarrays via a capillary-free fluid jetting mechanism, Proteomics, 5 (2005) 4138-4144.

[56] Sloane,A.J., Duff,J.L., Wilson,N.L., Gandhi,P.S., Hill,C.J., Hopwood,F.G., Smith,P.E., Thomas,M.L., Cole,R.A., Packer,N.H., Breen,E.J., Cooley,P.W., Wallace,D.B., Williams,K.L., Gooley,A.A., High throughput peptide mass fingerprinting and protein macroarray analysis using chemical printing strategies, Molecular & Cellular Proteomics, 1 (2002) 490-499.

[57] Pardo,L., Wilson,W.C., Boland,T.J., Characterization of patterned self-assembled monolayers and protein arrays generated by the ink-jet method, Langmuir, 19 (2003) 1462-1466.

[58] Roda,A., Guardigli,M., Russo,C., Pasini,P., Baraldini,M., Protein microdeposition using a conventional ink-jet printer, Biotechniques, 28 (2000) 492-496.

[59] Cai,Y.G., Ocko,B.M., Large-scale fabrication of protein nanoarrays based on nanosphere lithography, Langmuir, 21 (2005) 9274-9279.

[60] Valsesia,A., Colpo,P., Meziani,T., Lisboa,P., Lejeune,M., Rossi,F., Immobilization of antibodies on biosensing devices by nanoarrayed self-assembled monolayers, Langmuir, 22 (2006) 1763-1767.

[61] Yan,H., Park,S.H., Finkelstein,G., Reif,J.H., Labean,T.H., DNA-templated self-assembly of protein arrays and highly conductive nanowires, Science, 301 (2003) 1882-1884.

[62] Park,S.H., Yin,P., Liu,Y., Reif,J.H., Labean,T.H., Yan,H., Programmable DNA self-assemblies for nanoscale organization of ligands and proteins, Nano Letters, 5 (2005) 729-733.

[63] Sleytr,U.B., Huber,C., Ilk,N., Pum,D., Schuster,B., Egelseer,E.M., S-layers as a tool kit for nanobiotechnological applications, Fems Microbiology Letters, 267 (2007) 131-144.

[64] Juhasz,T., Djotyan,G., Loesel,F.H., Kurtz,R.M., Horvath,C., Bille,J.F., Mourou,G., Applications of femtosecond lasers in corneal surgery, Laser Physics, 10 (2000) 495-500.

[65] Maatz,G., Heisterkamp,A., Lubatschowski,H., Barcikowski,S., Fallnich,C., Welling,H., Ertmer,W., Chemical and physical side effects at application of ultrashort laser pulses for intrastromal refractive surgery, Journal of Optics A-Pure and Applied Optics, 2 (2000) 59-64.

[66] Vogel,A., Nonlinear absorption: Intraocular microsurgery and laser lithotripsy, Physics in Medicine and Biology, 42 (1997) 895-912.

[67] Tirlapur,U.K., Konig,K., Cell biology - Targeted transfection by femtosecond laser, Nature, 418 (2002) 290-291.

[68] Zeira,E., Manevitch,A., Khatchatouriants,A., Pappo,O., Hyam,E., Darash-Yahana,M., Tavor,E., Honigman,A., Lewis,A., Galun,E., Femtosecond infrared laser - An efficient and safe in vivo gene delivery system for prolonged expression, Molecular Therapy, 8 (2003) 342-350.

[69] Yanik,M.F., Cinar,H., Cinar,H.N., Gibby,A., Chisholm,A.D., Jin,Y.S., Ben Yakar,A., Nerve regeneration in Caenorhabditis elegans after femtosecond laser axotomy, Ieee Journal of Selected Topics in Quantum Electronics, 12 (2006) 1283-1291.

[70] Konig,K., Riemann,I., Fritzsche,W., Nanodissection of human chromosomes with near-infrared femtosecond laser pulses, Optics Letters, 26 (2001) 819-821.

[71] Watanabe,W., Arakawa,N., Matsunaga,S., Higashi,T., Fukui,K., Isobe,K., Itoh,K., Femtosecond laser disruption of subcellular organelles in a living cell, Optics Express, 12 (2004) 4203-4213.

[72] Denk,W., Strickler,J.H., Webb,W.W., 2-Photon Laser Scanning Fluorescence Microscopy, Science, 248 (1990) 73-76.

[73] Denton,M.L., Schuster,K.J., Rockwell,B.A., Accurate measure of laser irradiance threshold for near-infrared photo-oxidation with a modified confocal microscope, Journal of Microscopy-Oxford, 221 (2006) 164-171.

[74] Glickman,R.D., Johnson,T.E., Noojin,G.D., Stolarski,D.J., Denton,M.L., Kumar,N., Rockwell,B.A., Laser bioeffects associated with ultrafast lasers: Role of multiphoton absorption, Journal of Laser Applications, 20 (2008) 89-97.

[75] Rao,S.V., Anderson,K.W., Bachas,L.G., Oriented immobilization of proteins, Mikrochimica Acta, 128 (1998) 127-143.

[76] Kandere-Grzybowska,K., Campbell,C.J., Mahmud,G., Komarova,Y., Soh,S., Grzybowski,B.A., Cell motility on micropatterned treadmills and tracks, Soft Matter, 3 (2007) 672-679.

[77] Singhvi,R., Kumar,A., Lopez,G.P., Stephanopoulos,G.N., Wang,D.I.C., Whitesides,G.M., Ingber,D.E., Engineering Cell-Shape and Function, Science, 264 (1994) 696-698.

CHAPTER 2 *

NANOSCALE PROTEIN PATTERNING VIA NANO-IMPRINT LITHOGRAPHY

2.1 Introduction

In this chapter, we describe progress in developing a precise, high contrast, high resolution protein patterning technique using nanoimprint lithography (NIL) and surface chemical modification. NIL offers the advantages of high-throughput, low-cost, and high-reproducibility; and the capability of creating nanopatterns with features as small as 10 nm over large areas[2]. In NIL, a Si template, fabricated by e-beam lithography or other suitable techniques, is pressed against a polymer-coated substrate heated to above the glass transition temperature of the polymer. After cooling, the template is removed from the substrate, leaving an imprint of the template features in the polymer. To immobilize proteins, the patterned substrate is then modified sequentially with an aminosilane, biotin, streptavidin, and finally our choice of biotinylated target protein. In this paper we show that our technique yields nanopatterned proteins that retain their biological functionality, as demonstrated by antigen binding by patterned antibodies. This

* This chapter is reproduced, with minor modifications, from Hoff et. al.[1]

technique is compatible with protein patterning on both oxidized Si wafers, which may take advantage of the wealth of microfabrication techniques developed by the semiconductor industry for integrating immobilized proteins into bioMEMS devices, and optical quality coverglass suitable for microscopic analysis of protein distributions and interactions.

Many applications of patterned biomolecules can be enhanced by improving the resolution of the protein features. Smaller feature sizes enable, for example, the fabrication of high-density protein arrays for biosensors or proteomic screening; or facilitate studies of cellular interactions with small precisely located clusters of extracellular matrix proteins. A major advantage of the nanoimprint technique is that the features size can be reduced to the nanoscale to create high-density arrays, or potentially control placement of individual proteins, while still retaining high throughput and reproducibility. Most previous work in protein patterning has relied ultimately on conventional photolithography to form a base template for protein adsorption, and has thus been constrained to micron-scale resolution by the light diffraction limit[3]. Dip-pen lithography[4-6] and e-beam patterning[7;8] are capable of nano-scale resolution, but these are relatively delicate serial processes and thus lack scalability. NIL provides an alternative method of patterning substrates with resolutions down to sub-10nm, on the scale of individual protein molecules.

The most important criterion for any protein patterning technique is specific binding of target proteins, i.e. the technique must produce a high density of

biomolecules in desired regions (“patterned regions”) while preventing adsorption of these molecules in other regions (“unpatterned regions”). To satisfy this criterion we selectively passivate a substrate with a base pattern of an inert, nonpolar $(CF_x)_n$ (x = 1 or 2, n = number of monomer subunits, monomer MW = 31 or 50) polymer[9;10] coating to establish a template for the selective attachment of target linker molecules for highly specific covalent binding of biotin, which serves as a target for generalized protein binding through strong non-covalent biotin-streptavidin interactions.

2.2 Methods

Figure 2-1 schematically illustrates the patterning process. A silicon mold was fabricated by standard e-beam lithography and dry etching. To facilitate mold separation after imprinting the mold was coated with surfactant, perfluorochlorosilane **(Lancaster Synthesis, Windham, NH)** to provide a low energy surface. The material to be imprinted, poly(methylmethacrylate) or PMMA **(Aldrich, St. Louis, MO)** was spun onto a substrate of either 60nm thick silicon oxide thermally grown on silicon, or onto optical grade glass wafers (**Erie Scientific, Portsmouth, NH**). The PMMA was patterned by NIL: the mold and substrate were brought into physical contact at 175°C, and a pressure of 50kg/cm^2 was applied for 5 minutes before cooling to room temperature. After the mold and substrate were separated, O_2 reactive ion etching (RIE) was used to remove residual PMMA in the patterned regions (O_2 gas flow = 20 sccm, pressure = 20mTorr, power = 50W) and CHF_3 RIE was used to etch the newly

exposed oxide (CHF_3 gas flow = 40 sccm, O_2 gas flow = 5 sccm, pressure = 20mTorr, power = 150W), transferring the patterns to the oxide layer. In addition to etching away the exposed SiO_2 to the underlying Si substrate, this etching process deposits a thin passivating layer of CF_x polymer residue on the newly exposed Si surface[9;10]. The presence of this passivating polymer residue was verified by X-ray energy dispersive spectroscopy (XEDS). The remaining PMMA was then removed by sonication in acetone, leaving exposed SiO_2 regions separated by regions of CF_x passivated Si. Note that it is not necessary to etch down to the Si surface, as evidenced by the success of using the same fabrication procedure on glass substrate.

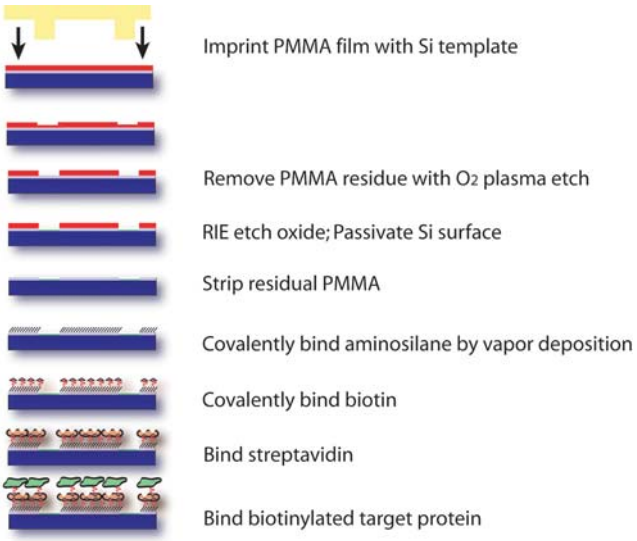

Figure 2-1: Process flow diagram of NIL substrate patterning and protein immobilization. Spin-coated PMMA polymer is patterned by NIL. Exposed SiO_2 regions are etched and a passivating $(CF_x)_n$ polymer (x = 1 or 2, n = number of monomer subunits, monomer MW = 31 or 50) is deposited during a CHF_3 RIE procedure. Residual PMMA is stripped away with acetone, exposing the underlying SiO_2 in the "patterned regions." An aminosilane monolayer is covalently attached to the exposed "patterned regions. Biotin-succinimidyl ester is then covalently linked to the primary amine of the aminosilane layer, and streptavidin is bound to the biotin layer. Finally, the biotinylated target protein is bound to the streptavidin layer.

The exposed oxide pattern selectively reacts with an aminosilane to form a covalently bound monolayer. We found aminopropyldimethylethoxysilane (APDMES, **SIA0603.0, Gelest, Morrisville, PA**) to be particularly effective. The single alkoxy group on the head of this silane ensures the reproducible deposition of a well-formed monolayer by minimizing unwanted self-polymerization[11-14]. Producing good silane monolayers on exposed silicon oxide or glass requires careful attention to procedure, especially with regards to temperature and humidity. NIL-patterned substrates were heated to 70˚C under dry nitrogen in a 0.4 liter glass chamber. 5µL APDMES was injected into the chamber through an airtight septum and allowed 20 minutes to react with the exposed SiO_2 surfaces before venting with fresh nitrogen for 90 seconds. Samples were then sonicated for 10 minutes in dry iso-octane, followed by ethanol, then 1mM NaOH to remove unbound silane from the surface and de-protonate the exposed amine. Deprotonation of the amine ensures the monolayer's reactivity to subsequent modifications by nucleophilic substitution reactions. The specificity of the aminosilane deposition was initially quantitatively verified by covalently binding tetramethylrhodamine succinimidyl ester (**C-1171, Molecular Probes, Eugene, OR**) to the amine tail group of the aminosilane monolayer via an n-hydroxysuccinimide reaction and measuring the resulting fluorescent intensities in the aminosilane patterned regions and the passivated Si regions. A very bright signal was observed in the aminosilane patterned regions, corresponding to a surface density of aminosilane on the order of a monolayer; no detectable fluorescent signal was detected on the passivated regions,

indicating the aminosilane does not react with the passivated Si surface. Therefore the plasma deposition of the fluoropolymer layer is responsible for the high differentiation between the two regions.

At this point, the APDMES-functionalized substrate is enclosed in a flow cell, 2.2cm long by approximately 50µm deep and 0.5cm wide, formed by fixing a glass cover slip to the top of 50µm thick aluminum foil spacers adhered to the substrate with vacuum grease. This allows sequential introduction of various buffers to the substrate, and also allows easy imaging using epifluorescence microscopy. Biotin is covalently bound to the exposed primary amine tail group of the patterned APDMES by filling the flowcell with a 68µM biotin-succinimidyl ester solution (**B-1513, Molecular Probes, Eugene, OR)** in 0.1M HEPES buffer at pH 7.65 for 20 minutes before flushing the flowcell with either deionized water or a biological buffer such as BRB80 (80 mM PIPES, 1 mM $MgCl_2$, 1 mM EGTA, brought to pH 6.8 with KOH). Next a streptavidin layer is deposited and bound to the biotin layer by flushing the flowcell with a 10µg/mL streptavidin solution in blocking buffer (0.1M HEPES, pH 7, containing 5mg/mL BSA) and incubating for 15 minutes. The resultant streptavidin monolayer serves as a base for the specific adsorption of any biotinylated target protein.

Biotinylated BSA served as our initial target protein. The target protein was bound by flushing the flowcell with a 50µg/mL biotinylated BSA solution in blocking buffer and incubating for 10 minutes. For fluorescent imaging, the heavily biotinylated BSA was further exposed to a 10µg/mL rhodamine-labeled

streptavidin **(S-870, Molecular Probes, Eugene, OR)** solution in Blocking Buffer for 10 minutes. The flowcell was rinsed with 0.1M HEPES, pH 7 containing an oxygen scavenging antifade cocktail (30mM glucose, 0.6 mg/mL glucose oxidase, 0.12 mg/mL catalase in BRB80) prior to transfer to the microscope stage.

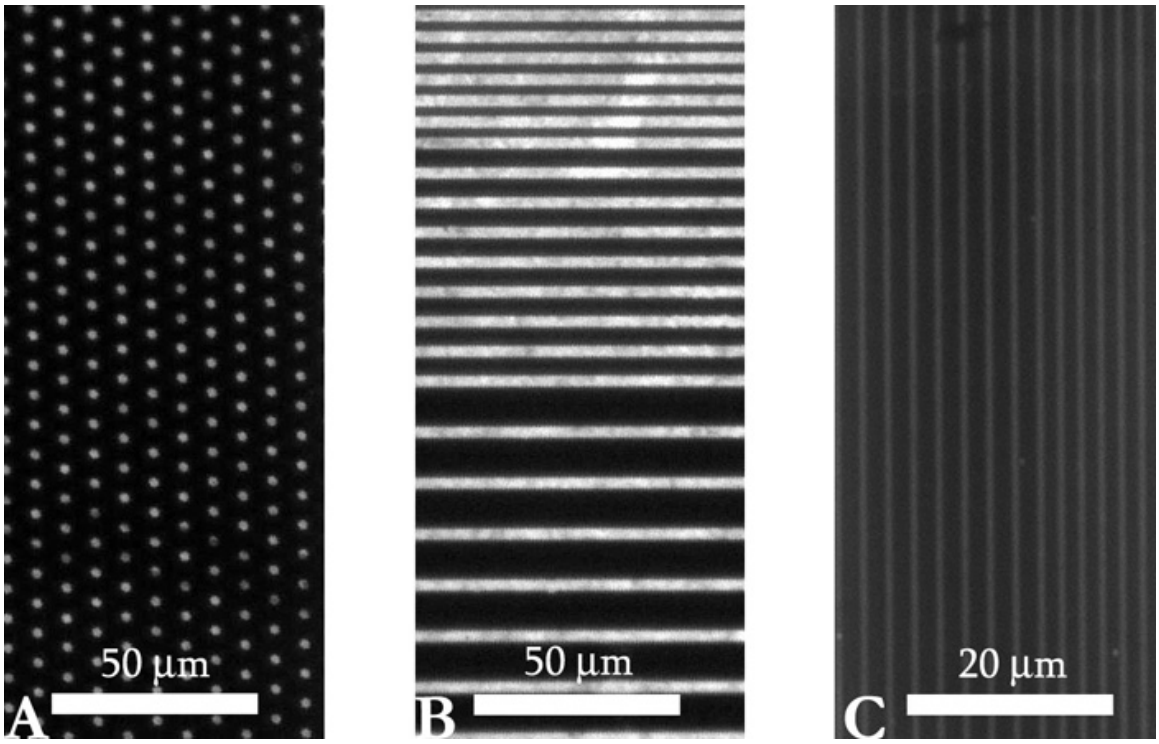

Figure 2-2: Epi-fluorescence image of microscale NIL patterning. Rhodamine-labeled streptavidin is bound to sharp uniform microscale dots (A) and lines (B) of biotinylated BSA protein on oxidized Si substrates. Fluorescent intensity signal in the passivated regions is at or below the noise level of the imaging system, indicating the fluorophore concentration in these areas is less than 0.1% of that observed in the patterned regions. C) Rhodamine-labeled streptavidin bound to patterns of immobilized biotinylated BSA on cover glass.

2.3 Protein Surface Density Estimation Using Quantitative Epi-Fluorescence

To quantify the surface density of target protein in the patterned regions we calibrated the measured fluorescent intensity of immobilized fluorescently labeled proteins to solutions of the same proteins at known concentration. Fluorescent images of patterned target proteins were captured on a Zeiss Axioplan 2 microscope fitted with a CoolSNAPcf CCD camera **(Roper Scientific, Trenton, NJ)**. The fluorescent intensity per molecule in the plane of focus was derived briefly as follows.

The total fluorescent intensity captured by the camera, I_C, imaging a flowcell of known depth is:

$$I_C = k_{CCD} I_E = k_{CCD} \int_z \int_r q N_F I_I(z) A(z) \phi(z,r) dr dz$$

where k_{CCD} is a constant relating the intensity of light incident on the camera's CCD chip to the camera's electrical signal, I_E is the total fluorescent emission captured, q is the quantum efficiency of the fluorophore, N_F is the concentration of fluorophore in solution, I_I is the intensity of the illuminating (excitation) light as a function of chamber depth z, A is the area of the illuminated field of view at depth z, and φ is the percentage of emitted light from each fluorophore that is captured by the objective lens at depth z and lateral distance r from the center of the image plane.

The illumination $I_I(z)$ can be expressed as:

$$I_I(z) = I_0 \frac{{r_0}^2}{(r_0 + z\tan\theta)^2}$$

where I_0 is the illumination in the plane of focus, r_0 is the illumination spot size in the plane of focus, and θ is half the angular aperture ($NA = n\sin\theta$).

In practice, a flowcell is formed by fixing a glass cover slip to the top of 50μm thick aluminum foil spacers adhered to the substrate with vacuum grease. A solution of blocking buffer (0.1M HEPES, pH 7, containing 5mg/mL BSA) is added to the flowcell to saturate the flowcell surfaces to prevent fluorophore from binding non-specifically. After about one minute, the flowcell is flushed with three flowcell volumes of a solution containing 5mg/mL BSA and a known concentration of the same fluorophore that was patterned on the sample of interest. The particular concentration of fluorophore varies by sample, and is chosen such that when imaged under conditions (illumination intensity, exposure time, etc.) identical to those used when imaging patterned sample of interest, the measured intensity lies within the dynamic range of the camera. Images of this calibration flowcell are then taken near the upper surface of the chamber immediately after imaging the patterned substrate, as the lamp intensity slowly drifts over time. To subtract off the background autofluorescence and camera dark current, another flowcell is fabricated and filled with blocking buffer. This flowcell is imaged similarly to the fluorescent calibration flowcell above. The intensity from this background sample is then subtracted from the intensity measured from the fluorescent calibration flowcell to get the experimental value for I_C. Because the imaging conditions and fluorophore used on the sample of

interest and fluorescent calibration flowcell are identical, many of the terms in the equation for I_C above can be lumped together, greatly simplifying the computation (e.g. k_{CCD}, q, I_0, and are the same in all samples). Considering potential errors stemming from geometric estimations (i.e. depth of the flowcell), light source instability, electrical noise, and reflectance of fluorophore emittance off of the SiO_2 substrate, we estimate the maximum error in this measurement to be approximately 30%.

This analysis shows a surface density of rhodamine-labeled streptavidin in the patterned region of approximately 120,000 molecules/μm^2, which is on the same order as the surface density expected from a close-packed streptavidin monolayer. Applying this analysis to the passivated Si region, we find the coverage of target protein in this region is undetectable, giving an upper limit of approximately 50 molecules/μm^2, or less than 0.1 percent of a monolayer. This demonstrates nearly complete monolayer coverage of target biomolecule in the patterned regions, with only a negligible amount of target protein adsorbed to the passivated regions.

2.4 Results and Discussion

One of the main advantages of using NIL technology in patterning is the ability to push the resolution to nanometer scales. To verify our ability to generate nanoscale protein patterns, we fabricated a mold to create 75 nm wide lines on Si substrates (Fig. 2-3). These nano-patterned substrates were prepared

identically to the micro-scale substrates, with biotinylated BSA as the target protein and rhodamine-labeled streptavidin subsequently bound for fluorescent imaging. The surface density measured by fluorescence is consistent with that observed on the micropatterned substrates, indicating an approximate monolayer of adsorbed target protein on the nanolines.

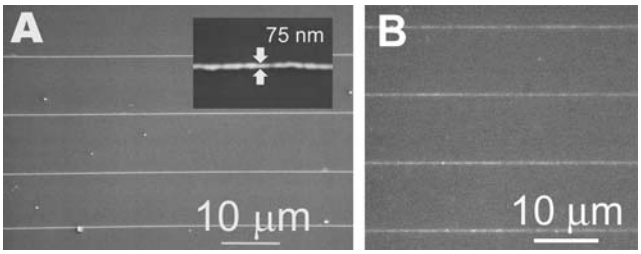

Figure 2-3: Proteins patterned onto sub-100nm features. (A) SEM image of oxide nano-lines formed on a Si substrate by NIL and RIE. **Insert**: Close-up SEM of oxide nano-line, showing a line width of less than 100nm. (B) Fluorescence micrograph of nano-lines after patterning with biotinylated BSA and binding rhodamine-labeled streptavidin. Analysis of the fluorescent intensity along the line indicates an approximate monolayer of target protein.

Broadly useful patterning technology requires that immobilized proteins retain their biological functionality. We have demonstrated that the functionality of patterned antibodies is retained by patterning the target protein goat anti-catalase **(ab6572, Novus Biologicals, Littleton, CO)**, and illustrating its binding of fluorescently labeled catalase from solution. Substrates were prepared as described above up to the streptavidin layer. A 10μg/mL solution of biotinylated anti-catalase in blocking buffer was then introduced into the flowcell for 10 minutes. The flowcell was flushed with HEPES pH 7.0, and a 50μg/mL solution of rhodamine-labeled catalase in blocking buffer was introduced. This solution

was incubated 10 minutes before rinsing with 0.1M HEPES pH 7.0 containing antifade. Fluorescent images show that the labeled catalase binds to the immobilized anti-catalase in the patterned regions (Fig. 2-4), while only a negligible amount binds in unpatterned regions. Quantifying the fluorescent intensity of the bound catalase as explained above yields a surface density of approximately 31,000 catalase molecules/μm^2, again on the order of a monolayer. One can easily imagine extending this technique to create ultra-high density antibody arrays for applications such as compact sensors and diagnostic devices, and for proteomic screening. The ability to specifically place small numbers of proteins molecules at desired locations will also benefit biophysical and molecular biology studies, as well as integration of protein activities into microscale devices (e.g. bioMEMS).

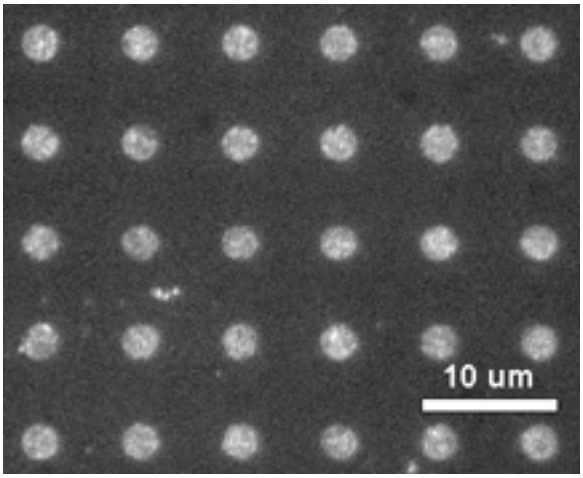

Figure 2-4: Epi-fluorescence image demonstrating the retained biological activity of patterned biomolecules. Biotinylated polyclonal anti-catalase antibody was patterned in 2μm dots, and the antibody's fluorescent antigen, rhodamine-labeled catalase, selectively binds to the antibody-patterned regions. The surface density of the bound catalase is approximately 31,000 molecules/μm^2.

In summary, we have developed a technique for immobilizing biomolecules with nanoscale resolution in a process that preserves functionality of the immobilized proteins. The use of nanoimprinting as the patterning method for the initial template enables high throughput ultra-high resolution patterning. Because our method relies on well-established and high affinity biotin-streptavidin binding, it can be applied to pattern virtually any protein, without the high degree of variability expected when protein is immobilized by virtue of more general chemical properties (i.e. hydrophobicity or charge). The target proteins bind specifically to the ligand patterns and the non specific adsorption is at least 1000-fold lower in the region of the passivation layer. We have demonstrated feature sizes down to 75nm, and since nanoimprinting allows for features as small as 10 nm across [2], we anticipate that placement of individual biomolecules will be possible. The compatibility of this technique with both SiO_2 substrates as well as optical quality cover glass broadens the potential applications of immobilized proteins, allowing easy integration with MEMS technologies as well as ready access to a wide range of optical imaging, measurement, and manipulation methods.

This versatile, highly specific, and biologically friendly technique for generating ultra-high resolution protein patterns will allow the diverse activities of proteins to be integrated into microfabricated devices and sensors. For example, protein chips, arrayed with a myriad of proteins, are becoming a useful tool in proteomics, enabling quick parallel screening of potential protein-protein interactions in large protein populations; as well as in more focused diagnostic

biosensors, concentrated on analysis of enzymatic interactions within a smaller set of proteins. When expanded to allow patterning of multiple proteins on a single substrate, the high contrast and resolution this technique provides will allow fabrication of chips with protein feature densities more than an order of magnitude greater than those currently available, potentially improving sensitivity, reducing required analyte volumes, and increasing the number of proteins that can be screened against on a single chip.

Reference List

[1] Hoff,J.D., Cheng,L.J., Meyhofer,E., Guo,L.J., Hunt,A.J., Nanoscale protein patterning by imprint lithography, Nano Letters, 4 (2004) 853-857.

[2] Chou,S.Y., Krauss,P.R., Zhang,W., Guo,L.J., Zhuang,L., Sub-10 nm imprint lithography and applications, Journal of Vacuum Science & Technology B, 15 (1997) 2897-2904.

[3] Blawas,A.S., Reichert,W.M., Protein patterning, Biomaterials, 19 (1998) 595-609.

[4] Liu,G.Y., Amro,N.A., Positioning protein molecules on surfaces: A nanoengineering approach to supramolecular chemistry, Proceedings of the National Academy of Sciences of the United States of America, 99 (2002) 5165-5170.

[5] Lee,K.B., Park,S.J., Mirkin,C.A., Smith,J.C., Mrksich,M. Protein Nanoarrays Generated By Dip-Pen Nanolithography. Science 295, 1702-1705. 4 A.D.
Ref Type: Generic

[6] Wilson,D.L., Martin,R., Hong,S., Cronin-Golomb,M., Mirkin,C.A., Kaplan,D.L., Surface organization and nanopatterning of collagen by dip-pen nanolithography, Proceedings of the National Academy of Sciences of the United States of America, 98 (2001) 13660-13664.

[7] Glezos,N., Misiakos,K., Kakabakos,S., Petrou,P., Terzoudi,G., Electron beam patterning of biomolecules, Biosensors & Bioelectronics, 17 (2002) 279-282.

[8] Harnett,C.K., Satyalakshmi,K.M., Craighead,H.G., Low-energy electron-beam patterning of amine-functionalized self-assembled monolayers, Applied Physics Letters, 76 (2000) 2466-2468.

[9] Coburn,J.W., Winters,H.F., Plasma-Etching - Discussion of Mechanisms, Journal of Vacuum Science & Technology, 16 (1979) 391-403.

[10] Oehrlein,G.S., Matsuo,P.J., Doemling,M.F., Rueger,N.R., Kastenmeier,B.E.E., Schaepkens,M., Standaert,T., Beulens,J.J., Study of plasma-surface interactions: Chemical dry etching and high-density plasma etching, Plasma Sources Science & Technology, 5 (1996) 193-199.

[11] Kallury,K.M.R., Macdonald,P.M., Thompson,M., Effect of Surface-Water and Base Catalysis on the Silanization of Silica by (Aminopropyl)Alkoxysilanes Studied by X-Ray Photoelectron-Spectroscopy and C-13 Cross-Polarization Magic-Angle-Spinning Nuclear-Magnetic-Resonance, Langmuir, 10 (1994) 492-499.

[12] Moon,J.H., Shin,J.W., Kim,S.Y., Park,J.W., Formation of uniform aminosilane thin layers: An imine formation to measure relative surface density of the amine group, Langmuir, 12 (1996) 4621-4624.

[13] Pallandre,A., Glinel,K., Jonas,A.M., Nysten,B., Binary nanopatterned surfaces prepared from silane monolayers, Nano Letters, 4 (2004) 365-371.

[14] White,L.D., Tripp,C.P., Reaction of (3-aminopropyl)dimethylethoxysilane with amine catalysts on silica surfaces, Journal of Colloid and Interface Science, 232 (2000) 400-407.

CHAPTER 3

REMOVAL OF PROTEINS FROM GLASS SURFACES USING FEMTOSECOND LASER IRRADIANCE

3.1 Introduction

In this chapter, we will describe the use of tightly focused ultrafast pulsed laser irradiance to remove adsorbed proteins from glass surfaces. This technique is capable of removing proteinaceous material with nanoscale feature size and placement with minimal collateral damage outside of the removal region, and without ablation of the underlying substrate. The procedure is simple, fast, and may be performed during experimental observation on standard microscope platforms. Ablation patterns are defined by the computer-controlled movement of a piezo-electric microscope stage. This allows arbitrary patterns to be ablated with rapid on-the-fly pattern generation. This in turn allows modification of a surface during the course of an experiment. For example, this protein removal allows *in situ* modification of a living cell's microenvironment during observation, as we demonstrate in Chapter 5 by guiding cell motility by selectively removing fibronectin from the surface near motile fibroblasts.

The use of tightly focused ultrafast laser irradiation to ablate extremely small features has been demonstrated in a range of materials, including dielectrics and, more recently, in biological materials. Irradiation using tightly focused ultrafast lasers has been shown to be capable of ablating dielectric materials with feature sizes well below the diffraction-limited spot size of the laser beam[1;2] via laser-induced optical breakdown (LIB). The technique has also been used to ablate biological materials, with diverse applications including ocular surgery[3-5], membrane poration[6;7], single neuron axotomy in C. elegans[8], and intracellular dissection of individual chromosomes[9] or mitochondria[10]. Many of these studies achieve ablation of biological materials at fluences significantly below the breakdown threshold for glass. This leads us to the proposition that we may remove biological materials from glass surfaces without damaging the underlying substrate. This could allow for the possibility of serial protein patterning of a large variety of proteins on a single substrate. Each newly cleaned surface may serve as an attachment site for a different type of protein, allowing the generation of surfaces with many spatially segregated surfaces coated with different proteins.

Additionally, the lack of ablation of the underlying substrate avoids potential complications one might otherwise encounter when performing experiments on irradiated surfaces. For example, surface ablation may worsen image quality if the sample is to be viewed by an optical microscopy modality, and changes in surface roughness due to ablation may directly affect cell behavior independent

of the effect of removing the protein from the surface. This chapter will demonstrate our success in achieving our objective of protein removal without ablation of the underlying glass substrate, and briefly discusses the potential mechanisms leading to this result. The mechanism is considered in further detail in Chapter 4. We will begin with a brief discussion of the mechanisms and effects associated with laser-induced optical breakdown.

3.2 Mechanism of Laser-Induced Optical Breakdown

Though our interest will lie primarily with the interaction of ultrafast laser pulses with biological materials and glass when the intensity is below the optical breakdown threshold for glass or water, we will briefly consider the mechanism of laser-induced optical breakdown (LIB) in dielectrics slightly above the breakdown threshold, as this is comparatively more well understood and easier to describe, and is instructive in the development of a description of the damage mechanisms in water or biological materials, which may be approximated to behave similarly to amorphous dielectrics with a similar effective bandgap, at intensities below the breakdown threshold[11;12]. Throughout this work, we will consider the breakdown threshold to refer to the minimum intensity or fluence at which material ablation is observed.

LIB occurs when incident laser irradiation excites large numbers of electrons into a free or quasi-free state, forming plasma in the focal region of the focused

beam. The free electrons now occupying the conduction band may then gain further energy through additional photon absorption, collisions with other excited electrons, and inverse Bremsstrahlung absorption, and ultimately the excited electrons' energy is transferred to heavy particles, heating the irradiated substance. At or above critical electron density, material ablation occurs. When using picosecond (ps) or longer pulse widths, electrons are predominantly excited by linear absorption of laser energy, limiting reproducible damage effects to the diffraction limited spot size of the laser and leading to relatively large amounts of energy being deposited in the vicinity of the damaged region[13]. This significant deposition of energy can cause a number of collateral damage effects outside the central damage region[14]. However, for sub-ps pulse widths, electron excitation is dominated by processes with a non-linear dependence on incident intensity, allowing critical free electron densities to be attained while the total energy absorbed is still relatively small, leading to damage due to plasma formation but only a relatively minor increase in temperature of the bulk substrate[13;15]. Because the total energy absorbed is relatively small, significantly less extensive collateral damage effects are observed near the ablated region.

During femtosecond laser damage, the electrons are excited initially by multi-photon ionization (MPI) and/or Zener tunneling, and these electrons serve as seeds for subsequent avalanche ionization. MPI occurs when a bound electron absorbs multiple photons before it can relax back to its ground state, such that

the total energy absorbed is sufficient to excite the electron into the conduction band[16]. In Zener tunneling, the electric field of the laser distorts the energy band structure to reduce the potential barrier, increasing the probability that an electron will escape from its potential well and become a free electron without directly absorbing a photon. MPI and tunneling are both highly non-linear processes, and thus extremely sensitive to incident intensity. This nonlinear relationship between intensity and electron excitation contributes to the deterministic character of generation of critical free electron densities characteristic of ultrafast ablation.

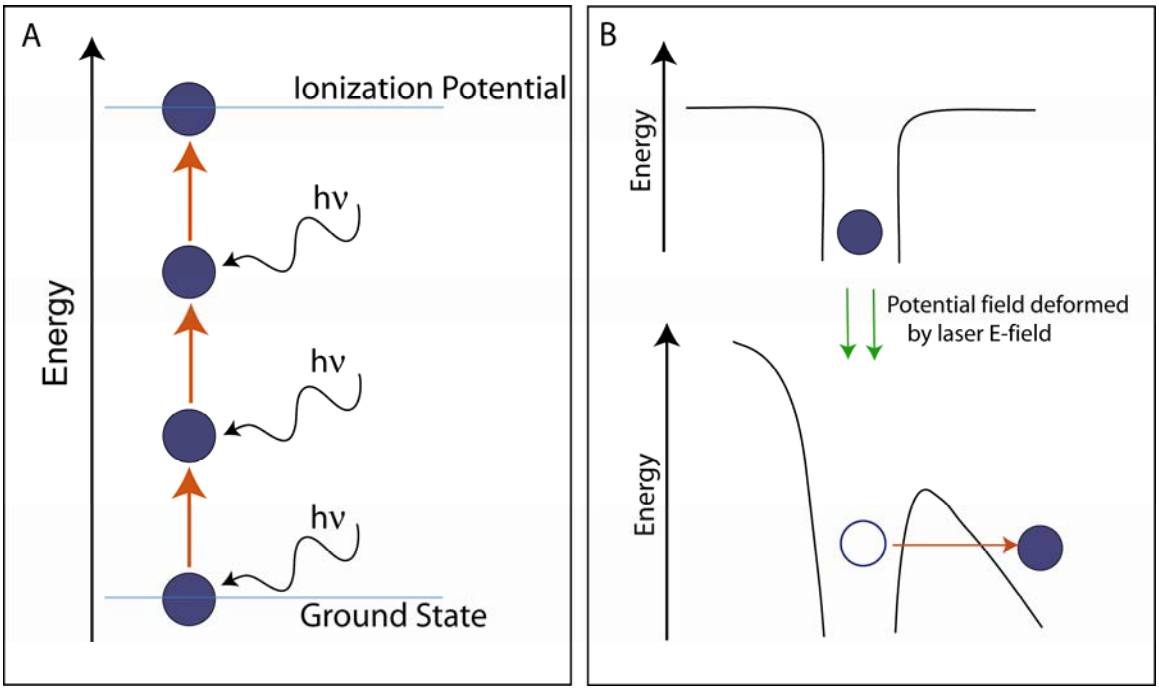

Figure 3-1: Nonlinear laser-induced electron excitation mechanisms. A) In multiphoton ionization, an electron in a ground state quickly absorbs photons whose total energy exceeds the band gap, before the electron can relax back to its ground state. B) In Zener tunneling, the intense electric field at the laser focus distorts the potential field felt by the electron, allowing it to move into the conduction band without directly absorbing a photon.

This determinism is further supported by the insensitivity of free electron densities to native carriers in the irradiated substrate. When using longer pulses with lower intensity, avalanche ionization is largely seeded by these carriers already present in the material. Because these native carriers may be sparsely or irregularly distributed, this leads to less deterministic breakdown. In contrast, sub-picosecond pulses generate orders of magnitude more seed electrons through MPI and tunneling. Because the seed electrons are generated by the laser pulse, critical densities of free electrons are attained largely independent of the distribution of native carriers in the substrate[13].

The deterministic generation of critical free electron densities using ultrafast pulses allows the ablation of features significantly below the diffraction-limited spot size of a tightly focused beam[1;2]. Figure 3-2A depicts a cross-section of a Gaussian intensity profile expected across from such a beam. Although the detailed mechanisms of the ablation process are still being investigated, there is broad agreement on the general features of the mechanism. Electrons are excited to critical density only in the region of the profile which exceeds the breakdown threshold of the irradiated material. Outside this region, only relatively small numbers of free electrons are generated, whose total energy content is small enough to dissipate non-destructively. This gives rise to well-confined ejection of material within the breakdown region while incurring negligible collateral damage outside of the breakdown region. As demonstrated

in Figure 3-2B, a volume of material far smaller than the focal volume has been removed, with minimal collateral damage in the surrounding region.

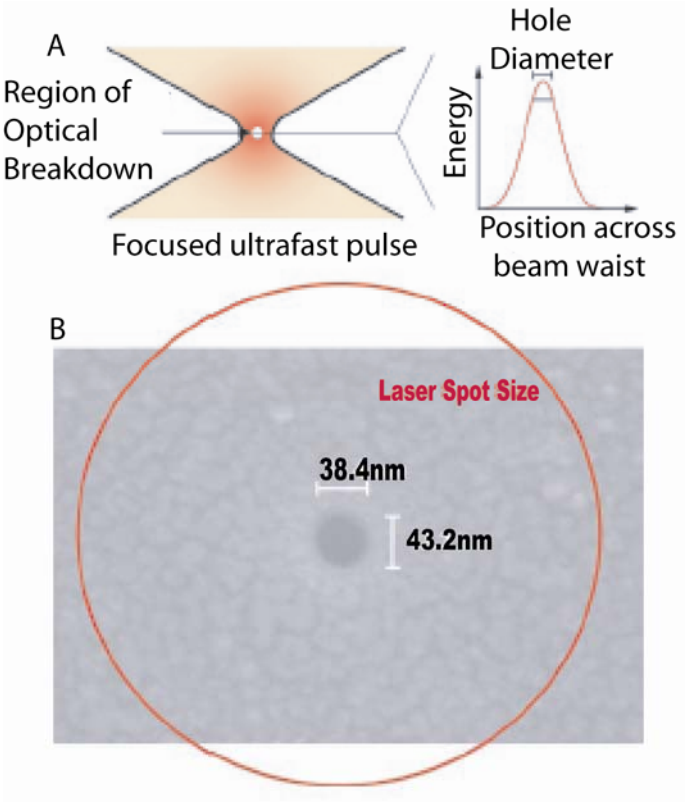

3-2: LIB of an area much smaller than the laser's spot size. A) Schematic of a tightly focused ultrafast beam with a gaussian intensity profile. The intensity only exceeds the critical intensity in the center of the intensity profile, allowing the ablation of features smaller than the diffraction limited spot size. B) An example of nanoscale ablation of glass. The red circle indicates the $1/e^2$ spot size of the laser beam waist. Figure adapted from Joglekar et al.[2]

3.2.1 Sub-threshold Ultrafast Laser Irradiation Effects

As compared to investigations of ablation at and above critical intensity, relatively little research has addressed the effects and mechanisms of irradiation with ultrafast pulses at sub-threshold intensities, in which critical free electron densities are not achieved. While irradiance at or above critical intensity results

in obvious material removal within the damaged region, sub-threshold effects are more subtle. The lack of attention given to sub-threshold effects can be attributed largely to the minimal changes they incur and the difficulty in characterizing those effects.

As noted in the previous section, due to the highly non-linear dependence of electron excitation on irradiation intensity, only a relatively small number of free electrons are excited below the critical threshold intensity and little energy is deposited in the irradiated substrate during the short pulse length. Although it has been inferred that high-density plasmas are not generated and material ablation is not observed under these conditions[1;17], the low-density plasmas generated can still cause significant chemical, thermal, and mechanical effects on the irradiated region.

For example, in solid dielectrics, it has been observed that sub-threshold irradiation can result in material densification, change in refractive index[18], generation of color centers, and so-called dry laser cleaning of surfaces[19-21]. These changes can largely be attributed to the observation that the threshold for melting is lower than the material removal threshold[22;23]. In biological materials, sub-threshold pulses have been shown to damage DNA[24], sever biological filaments such as microtubules or actin[25;26], or disrupt cell membrane continuity[6;27]. In the following sections, we will consider the origin of the damaging chemical affects, heating, and/or acoustic stresses generated by

low-density plasmas, with particular attention to their effects on biomolecules in aqueous media.

3.2.2 Chemical Effects

Free electrons in biological media can generate damage by several broad mechanisms. First, they can interact with water molecules to generate reactive oxygen species (ROS), including OH* and H_2O_2[16]. Such ROS are highly reactive and well-known to cause damage in biological materials. Second, the free electrons may interact directly with biomolecules, resulting in bond cleavage or rearrangement. Third, an electron within a bond itself may be excited, leading to cleavage of the associated bond. The exact nature of the interaction of low-energy electrons in bond breakage in biological media is not well understood, but it has been observed that electrons with energies as low as a few eV can generate breaks in DNA strands[28;29] and damage the peptide backbone of proteins[30] [31].

It should be noted that although proteins have negligible linear absorption at visible wavelengths, in particular at the wavelength of the laser light used in the experiments described in chapters 3 and 4, 527nm, most proteins do exhibit significant absorption at ultraviolet wavelengths, centered at 280nm, due primarily to aromatic rings in the amino acid tryptophan. It is thus possible for electrons within the protein to be excited directly by 2-photon absorption. This

provides a mechanism to affect protein damage independent of the generation of free electrons from the bulk aqueous media.

3.2.3 Thermal Effects

As the excited electrons collide with heavy particles or non-radiatively recombine, heat is generated in the irradiated volume. The time constant for electron cooling through collisions with heavy particles is on the scale of a few ps[32], while for low-density plasmas such as those generated by sub-threshold pulses the time constant for recombinative processes is expected to be tens of ps[33]. This implies that the maximum temperature resulting from a pulse will be reached somewhere between a few and tens of ps for a sub-threshold pulse.

An upper bound for the temperature rise in the irradiated region can be estimated based on the total energy absorbed in the focal volume. As noted above, negligible energy is transferred from electrons to heavy particles during a femtosecond pulse. Because the electron cooling times are much longer than the pulse length, the energy deposited into the irradiated region can be evaluated simply as the number of free electrons generated during the pulse multiplied by the mean energy gain of each electron. If we assume that each electron exceeding ΔE produces another free electron through collisions[33;34] then the average energy gain per electron will be ΔE /2. Thus, the plasma energy density is

$$\varepsilon = \frac{3}{2}\rho_{\max}\Delta E$$ [35]

And the change in temperature is simply $\Delta T = \varepsilon / C_p$, where C_p is the heat capacity of the medium.

Of particular importance for biological media is the achievement of temperatures over 100C. At these temperatures, proteins are likely to thermally denature, resulting in a loss of physiological function due to misfolding. As the increase in temperature is transient, though, and dissipates quickly, it is possible that in this case the achievement of 100C temperatures will not directly result in protein denaturation.

When using high repetition rates, it is possible that the thermal energy does not have time to dissipate completely between pulses. In most studies of sub-threshold damage in biological media, damage was observed after hundreds or thousands of sub-threshold pulses at repetition rates near 80MHz[6;24-27]. In this case, thermal energy can be incubated, leading to temperature increases from a series of pulses much greater than the temperature achieved as the result of a single pulse[35]. In our experiments, the repetition rate is kept low, 2kHz, allowing us to neglect incubation of thermal energy between pulses.

3.2.4 Acousto-Mechanical Effects

The acoustic transit time across the focal volume of the laser pulse (1.3NA, 527nm) is hundreds of picoseconds, at least an order of magnitude longer than the thermalization time. The increase in temperature will then generate an increase in pressure in the focal volume which cannot be mediated by acoustic relaxation. The initial pressure after thermalization can be expressed as

$$p_0(r) = \Gamma \varepsilon(r)$$

This high-pressure region in the beam focus then relaxes into the surrounding area, generating a compressive shock wave followed by a tensile stress in its wake. If this tensile stress exceeds the tensile strength of water,approximately 300bar, a bubble will be formed[35]. Bubble formation has been used as an experimental criterion for optical breakdown in aqueous media[36;37]. However, it is possible that material damage may result from the mechanical stress effects below this critical bubble formation threshold.

3.2.5 Summary

LIB is capable of material removal with resolutions far smaller than the diffraction limited spot size due to its highly non-linear mechanism of free electron generation. Damage may also be induced in condensed matter at laser fluences considerably below the critical threshold, however, by a variety of mechanisms, notably through chemical, thermal, and acoustic effects.

The exact nature of sub-threshold damage mechanisms in biological media are not well-understood. In the remainder of this chapter and through chapter 4, we will explore the effects of this sub-threshold damage by irradiating the interface between glass and biological media. These studies lend some insight into the mechanism of sub-threshold damage and point towards some potential applications of irradiated glass surfaces.

3.3 Irradiation of Protein-Coated Surfaces Decorated with Microtubules

We begin this inquiry with a simple experiment, adsorbing biotinylated BSA and streptavidin to a glass coverslip followed by biotinylated microtubules (MTs), irradiating regions of the coverslip, and examining both the resulting distribution of BSA in the irradiated regions and the damage done to MTs which lie in the region of irradiation. MTs are rigid hollow cylindrical biological structures, approximately 25nm in diameter[38] and with a persistence length of hundreds of microns[39]. We chose to examine damage incurred by MTs, as their rigid and regular structure provides a convenient scaffold from which to examine collateral damage to biological structures in the vicinity of the laser focus. We are especially interested in the effects of relatively low intensity pulses, below the glass ablation threshold. Atomic force microscopy (AFM) was used to examine the irradiated surface, as this technique is sufficiently sensitive to resolve the distribution of proteins on a surface[40].

3.3.1 Methods

3.3.1.1 Optical setup

All experiments described in chapter 4 and 5 were performed using a chirped-pulse amplified (CPA) Nd:glass ultrafast laser with a pulse duration of approximately 500fs. The laser pulse is frequency doubled with a KTP crystal to 527nm wavelength. The laser beam is then input into a Zeiss Axiovert 200 inverted microscope collinear with the epifluorescence beam path, entering the back aperture of the objective. The collimated beam overfills the back aperture of the objective such that $1/e^2$ diameter of the beam is approximately the back aperture diameter. A MadCity MCL 01075 piezo-driven nanostage is attached to the microscope stage, allowing for nanoscale precision stage movement. See Figure 3-3 for a schematic of the optical setup.

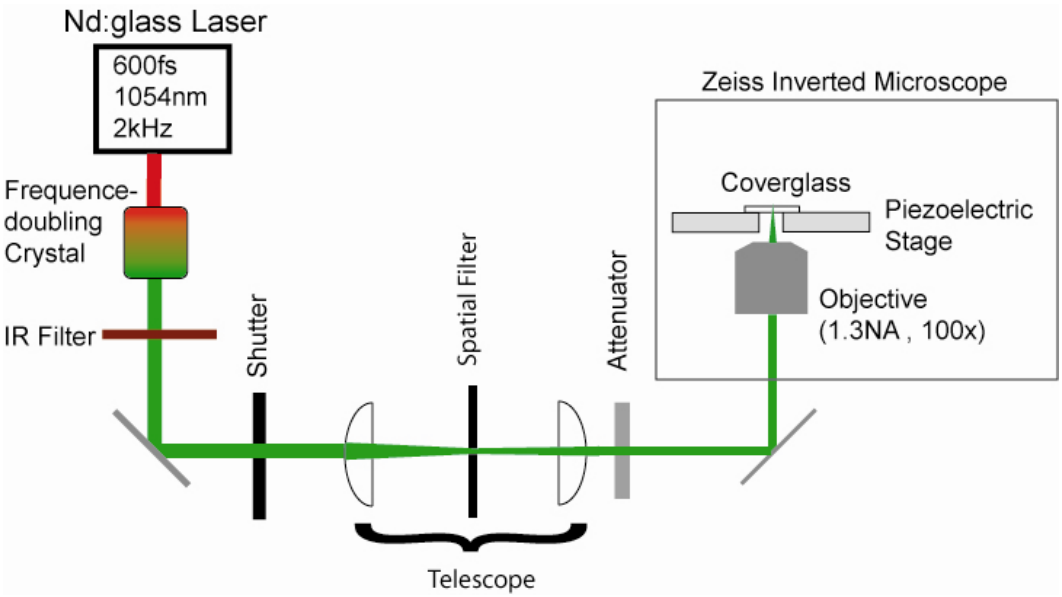

Fig. 3-3: Optical setup used in these experiments. A CPA Nd:glass laser is frequency doubled through a KTP crystal, focused into a spatial filter to clean up the beam shape, and attenuated before entering a Zeiss inverted microscope.

3.3.1.2 Flowcell preparation and protein adsorption

Flowcells were constructed from a standard microscope slide and coverslip, separated by double-sided sticky tape (of approximately 100um thickness). This flowcell was loaded by capillary action, with a solution containing 100ug/mL biotin-labeled BSA in PBS. This solution was allowed 5 minutes to interact with the flowcell surfaces before being rinsed by flowing 100uL (approximately three flowcell volumes) PBS through the flowcell. 50ug/mL streptavidin in PBS was loaded and again allowed to interact for 5 minutes before a solution containing stabilized microtubules (MT), as described below, was introduced for five minutes. The flowcell was then flushed with PBS and sealed with VALAP.

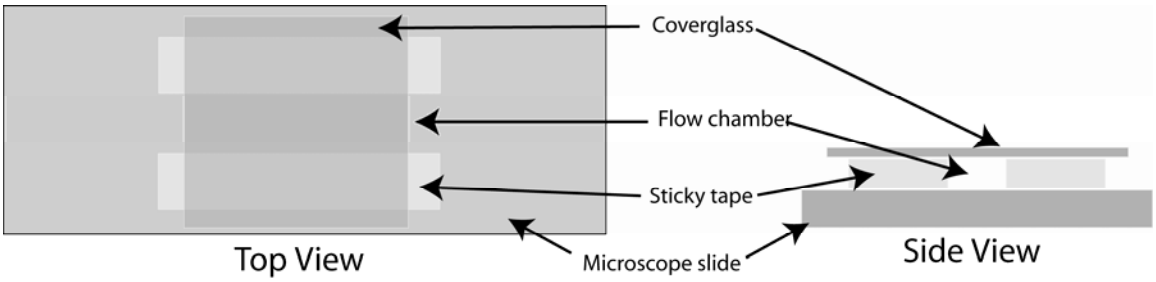

Figure 3-4: Schematic of a flowcell. A coverglass is affixed to a standard microscope slide using two strips of double-sided sticky tape. Fluid is loaded into the central channel by capillary action.

3.3.1.3 Biotinylated Microtubule Preparation

3mg/mL tubulin in Brinkley Buffer (BRB80) buffer was brought to 1mM $MgCl_2$ and 1mM GTP. This solution was incubated 15 minutes at 37C. The resulting MT-containing solution was then stabilized by adding taxol to 10uM. The solution

was pelleted in a Beckman airfuge for 5 minutes and resuspended in BRB80 with 10uM taxol and 20uM biotin-XX-SE. This solution was incubated 10 minutes at 37C before quenching the reaction with 4mM glycine. This solution was kept 10 minutes at room temperature before pelleting again in the airfuge for 5 minutes. The MT pellet was resuspended in BRB80 and 10mM ethylene glycol disuccinate bis(sulfo-N-succinimidyl) ester (EGS) was added to cross-link the microtubules. This solution was incubated at 37C for 10 minutes before quenching the reaction with 4mM glycine. The MTs were again pelleted in the airfuge and resuspended in BRB80. This solution was diluted 10-fold in BRB80 before introducing into the flowcell.

3.3.1.4 Ablation

The sample was then mounted on a Zeiss Axiovert 200 microscope and imaged with a 100x 1.3NA oil immersion NeoFluor objective. The laser was scanned in single lines across the surface, with the axial height of the focus varied so as to ensure the beam intercepts the coverslip surface for some portion of the travel (See Figure 3-5). The stage velocity was controlled such that the spacing between pulses was roughly 125nm, approximately half the radius of the beam waist. The pulse energy was varied from 2.2nJ to 7.4nJ, such that the fluences tested ranged between approximately 1.2 J/cm^2 and 4 J/cm^2.

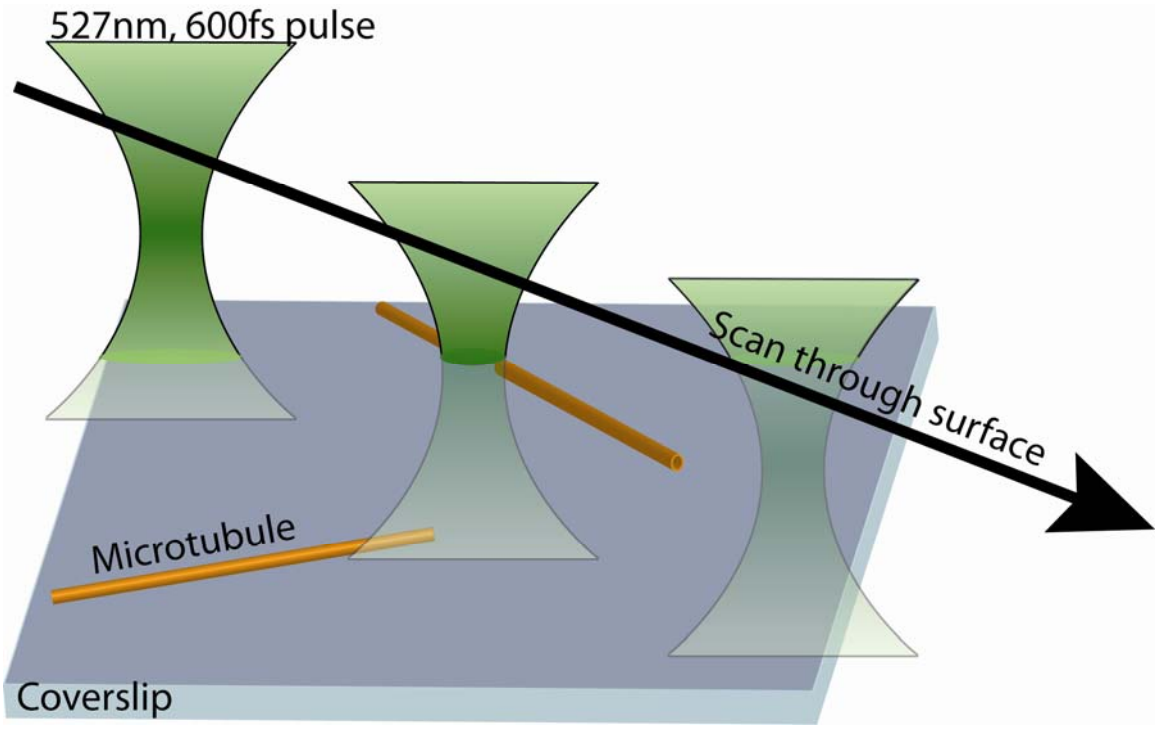

Figure 3-5: Depiction of laser scanning through the surface as performed in experiments described in sections 5.2 and 5.3. The laser is simultaneously scanned laterally across the surface and axially through the surface to ensure that the beam intersects the surface for some portion of its travel. The surface is shown decorated with microtubules.

3.3.1.5 Excision and dehydration:

After laser ablation, the coverslip outer surface (which had been directed towards the microscope objective during irradiation) was cleaned alternately with acetone- and ethanol-soaked KimWipes, until no residue of immersion oil visible to the naked eye remained. The bulk of the VALAP sealing the ends of the flowcell was removed with a razor blade. The flowcell was then submerged in a dish containing phosphate buffered saline (PBS) to ensure that the surface remained hydrated during excision. Using a diamond-tipped scribe and non-abrasive tweezers, a portion of the coverslip containing the ablated region was

removed. Care was taken to ensure that the excised portion did not come into contact with ethanol-soluble contaminants, namely VALAP, tape adhesive, and immersion oil. The excised coverslip portion was transferred to a dish containing 25% EtOH, and gently agitated for 3 minutes. The fluid was aspirated and replaced subsequently with 50%, 75%, 85%, 95% EtOH, and thrice with 100% EtOH (maintained with Type 3A molecular sieves, Fisher Scientific # MMX1583A1), gently agitating for 3 minutes at each concentration. During each aspiration, enough fluid was left in the dish to ensure that the coverslip did not dry prematurely. The final rinse of EtOH was aspirated and the dish was loosely covered with lint-free paper to minimize contamination, and the coverslip to air-dry overnight. The coverslip portion was then mounted on a standard AFM stub.

3.3.1.6 Imaging:

The sample was imaged via tapping mode atomic force microscopy (AFM) using a Digital Instruments Nanoscope IIIa Scanning Probe Microscope, using a MULTI75AL AFM probe, with tip radius specified to be less than 10nm.

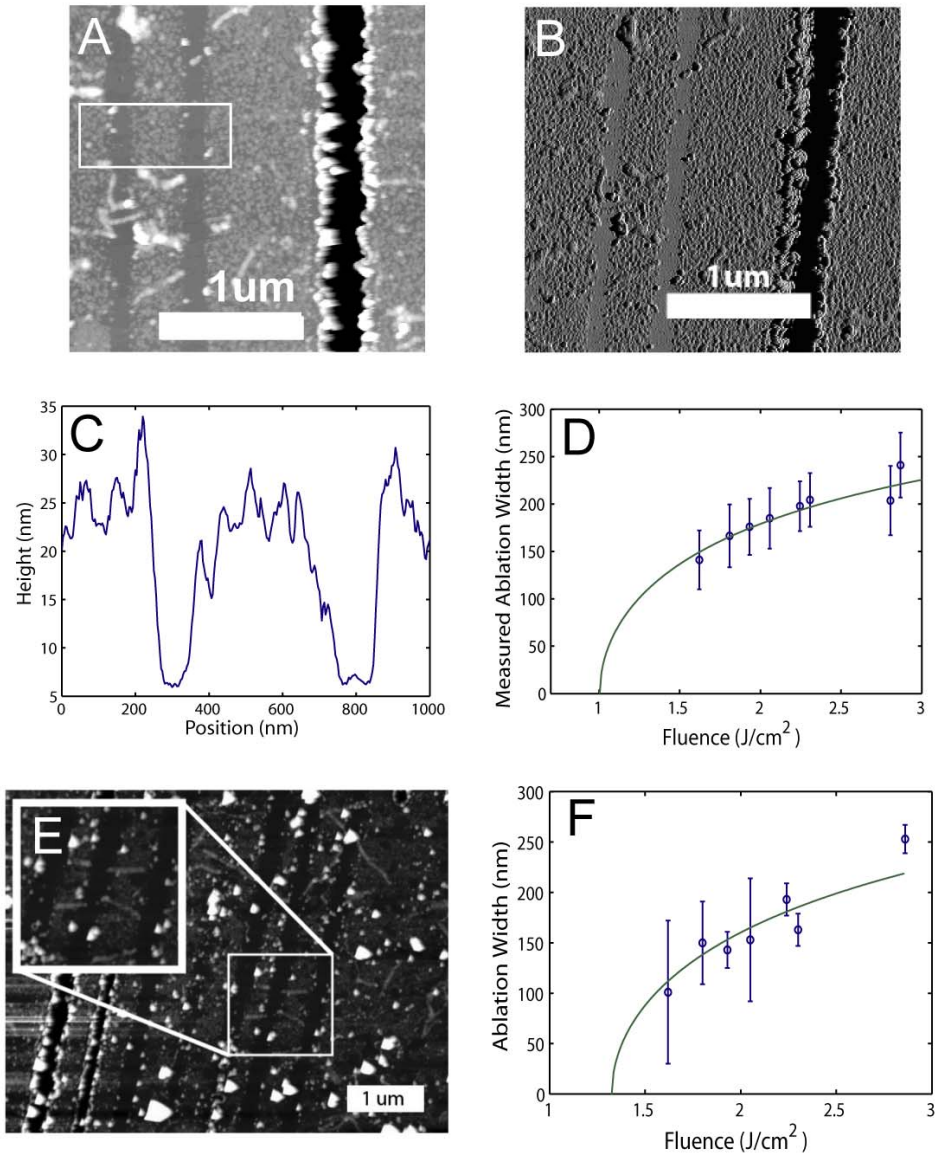

Figure 3-6: Damage of irradiated immobilized proteins. A) Height map of an irradiated region imaged via AFM. Three damage tracks are shown. Note the lowering and smoothing in the two irradiation tracks on the left. The right-most damage track was irradiated above the glass breakdown threshold. The white box indicates the region corresponding to the averaged profile in panel C. B) AFM phase image of the same region shown in A. The lowering and smoothing of the phase response in the irradiated regions indicates a harder, less sticky surface. C) Averaged height profile for the region in the white rectangle in A. D. Measured width of protein removal from the surface as a function of fluence. The data is fit to an inverse Gaussian, giving a threshold fluence of 1±0.033 J/cm^2. E) AFM image of irradiated damage tracks intersecting microtubules. Inset magnifies two microtubule damage points. F) Measured width of damage done to microtubules. A fit to an inverse Gaussian gives a threshold estimate of 1.3±0.33 J/cm^2.

3.3.2 Results

Examination of AFM images the revealed significant differences in the height and smoothness of the irradiated lines as compared to un-irradiated regions. For laser fluences above 3.1J/cm^2, it is apparent that the irradiated lines are significantly smoother than un-irradiated regions (see Figure 3-5A-C). This effect was quantified using the rms surface roughness, R_q:

$$R_q = \sqrt{\frac{1}{MN}\sum_{i=1}^{N}\sum_{j=1}^{M} z^2(x_i y_j)}$$

where M and N are the dimensions of the area to be analyzed, and z(x,y) is the measured height of each pixel. Such analysis reveals that unablated regions have a mean height of approximately 25nm and a roughness of approximately 10nm, while ablated regions have a mean height of approximately 5nm with roughness of less than 5nm, similar to that of an unmodified bare coverslip surface. Note that there appears to be a sharp boundary between the smooth ablated regions and the relatively rough un-irradiated regions, and that the ablated lines have a consistent width. Such sharp boundaries and consistent widths imply a deterministic non-linear mechanism for protein damage or removal.

To quantify the distribution of widths of the smoothed regions where proteins have presumably been removed, AFM images of the irradiated lines were sectioned into approximately 200nm long segments. The average width of the

line in each segment was recorded. Figure 3-6D shows the relationship between measured width and incident laser fluence. Note that for fluences below 1.6J/cm^2, removal of proteins (i.e. smoothing of the surface in the region which was illuminated by the laser focus) was not apparent, and that for fluences above 2.8J/cm^2, the underlying glass was damaged, obscuring the smoothing phenomenon characteristic of protein ablation.

To extrapolate the damage threshold F_{th}, we fit the above data to an inverse Gaussian, which is the expected dependence for highly non-linear damage resulting from a beam with a Gaussian profile,

$$D = \sigma\sqrt{\ln\frac{F_a}{F_{th}}} \quad [41]$$

where D is the width of the line, F_a is the incident energy, and σ and the the threshold fluence F_{th} are fitting parameters. The fitting parameter σ describes the beam shape and diameter. For a Gaussian point spread function, it will be equal to $\sqrt{\frac{D_0^2}{2}}$, where D_0 is the standard deviation. Such a fit gives a threshold fluence of 1.0±0.033 J/cm^2 and σ=76±2.37nm. Though the small experimental space available for sampling (e.g. fluences roughly between 1.6 and 3 J/cm^2) limits the predictive power of this fit, the extrapolated threshold broadly agrees with other published work [26].

We also measured the width of MTs severed by irradiation. MTs have a rigid, regular structure, and thus provide a useful scaffold with which to evaluate the

extent of collateral damage, as well as the minimum ablation feature size. MTs were clearly severed where the irradiation lines intersected MTs immobilized on the surface, as shown in Figure 3-6E. The width of the removed section of a MT was recorded along with the pulse energy. Note that the variance of these features is considerably greater than that obtained when measuring the width of the smoothed surface in the previous section. This variation can be explained largely by the geometry of the setup. The MTs lie on top of the surface, but are not in-plane with the surface. They may stand off from the surface a small and variable distance, such that each severed MT may lie in a slightly different focal plane. Additionally, after severing, even a small acoustic shock wave generated in the laser focus may move the MT tips somewhat, before possibly re-binding to a different set of streptavidin molecules. The shape of some severed MT tips indicate that this likely occurred, as it appears that near the irradiated region, the MTs flex or curl.

The relationship between feature size, in this case, the width of the removed MT section, was again fit to an inverse Gaussian as in the previous section. Due to the increase in variance noted above, the fit is less compelling than the fit of protein removal from the surface (see Figure 3-6F). However, the solution gives an estimated threshold fluence F_{th}=1.3±0.33J/cm^2 and σ = 88±28.3nm, which agree well with the threshold energy and spot size calculated based on removal widths of protein from the surface described above.

3.4 Estimation of Removal Width by Fluorescence Microscopy

We also estimated the area of the protein removal region as a function of pulse energy by rastering the laser across an antibody-coated surface, with varying spacing between the rasters. After introducing the fluorescent antigen, the relationship between fluorescent intensity in the irradiated region and the inter-raster spacing reveals information about the extent of protein removal.

3.4.1 Method

3.4.1.1 Flowcell preparation and protein adsorption

Two holes were drilled in standard microscope slides using 1mm diameter diamond-tipped drill bits. The slides were cleaned with Alconox detergent. 100uL pipet tips were inserted into the holes and the interface sealed with RTV silicone sealant. These tips serve as an inlet and outlet for buffer exchange during observation on the microscope. Flowcells were then constructed from this modified microscope slide and a coverslip, separated by double-sided sticky tape (of approximately 100um thickness).

We introduce 50ug/mL biotin-labeled BSA into the flowcell for 5 min, then rinse with 500ug/ml un-labeled BSA.

3.4.1.2 Ablation

We rastered a tightly focused ultrafast pulsed laser across the coverslip surface, illuminating a series rectangular patches. The fluence and/or inter-raster spacing was varied between patches (see Figure 3-7). Pulses were placed such that the interpulse spacing is approximately half the expected focus spot diameter.

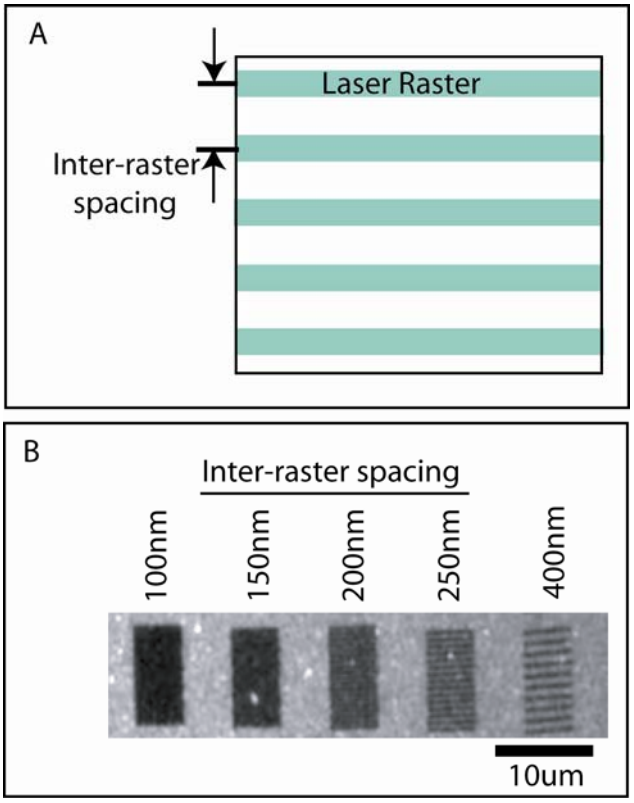

Figure 3-7: Schematic of laser raster spacing. In the experiments described in section 4.3, regions of a protein-coated surface are irradiated by rastering the laser across the region. The inter-raster spacing is varied as shown.

3.4.1.3 Imaging

After ablation, 20ug/mL FITC-labeled streptavidin in PBS with 500ug/mL BSA was introduced as a reporter molecule for 10 minutes before flushing with antifade. The irradiated regions were imaged using epifluorescence microscopy.

3.4.2 Results

In analyzing the results of this assay, we assume that once the inter-raster spacing is equal or less than the protein removal width, the fluorescent intensity in that region will not decrease significantly with further decrease of inter-raster spacing. From this rationale, we can place an upper bound on the removal width for a particular fluence as the lowest inter-raster spacing for which the fluorescent intensity is statistically different from the intensities from patches irradiated with smaller inter-raster spacings (see Figure 3-7).

Figure 3-8 illustrates the results of this analysis. Figure 3-8C shows the upper bound for the damage width, determined as described above. The upper bounds for the line widths determined in this assay are significantly smaller than the removal widths observed by AFM in section 4.2. It is possible that this discrepancy arises as a consequence of undamaged molecules immobilized in the interstices between damage regions. Though the distance between pulses within a raster is not systematically varied in our studies, the area of the damage

spot will be smaller at lower fluences, leading to less overlap in the damage regions. With insufficient overlap of damage between pulses, the damage region for each raster is no longer appropriately approximated as a rectangular damage area, as was depicted in Figure 3-7A. Figure 3-8A illustrates the consequences of this observation. The spacing between rasters necessary to totally remove protein from the surface is significantly less then the apparent damage width measured using AFM. It would be interesting to image a sample prepared in precisely this manner, with line spacing between rasters decreasing to approximately 30nm, under AFM for comparison.

Additionally, the shapes of the curves in Figure 3-7B deviate significantly from what one expects from a deterministic removal process. If the damage is deterministic, we expect a linear dependence of fluorescent intensity on irradiation line spacing, e.g. if the number of laser rasters is doubled by halving the line spacing, then the amount of protein removed should also double.. Instead, at low fluences we see an asymmetric sigmoidal relationship, e.g. $F = F_{\max} \exp(-b * \exp(-kd))$, where *F* is the observed fluorescent intensity, F_{max} is the maximum fluorescent intensity observed, *d* is the line spacing, and *b* and *k* are fitting parameters. The fluorescent intensity *F* is presumably proportionate to the surface density of protein remaining after irradiation. This asymmetric sigmoidal dependence on line spacing may imply a non-linear probabilistic damage mechanism.

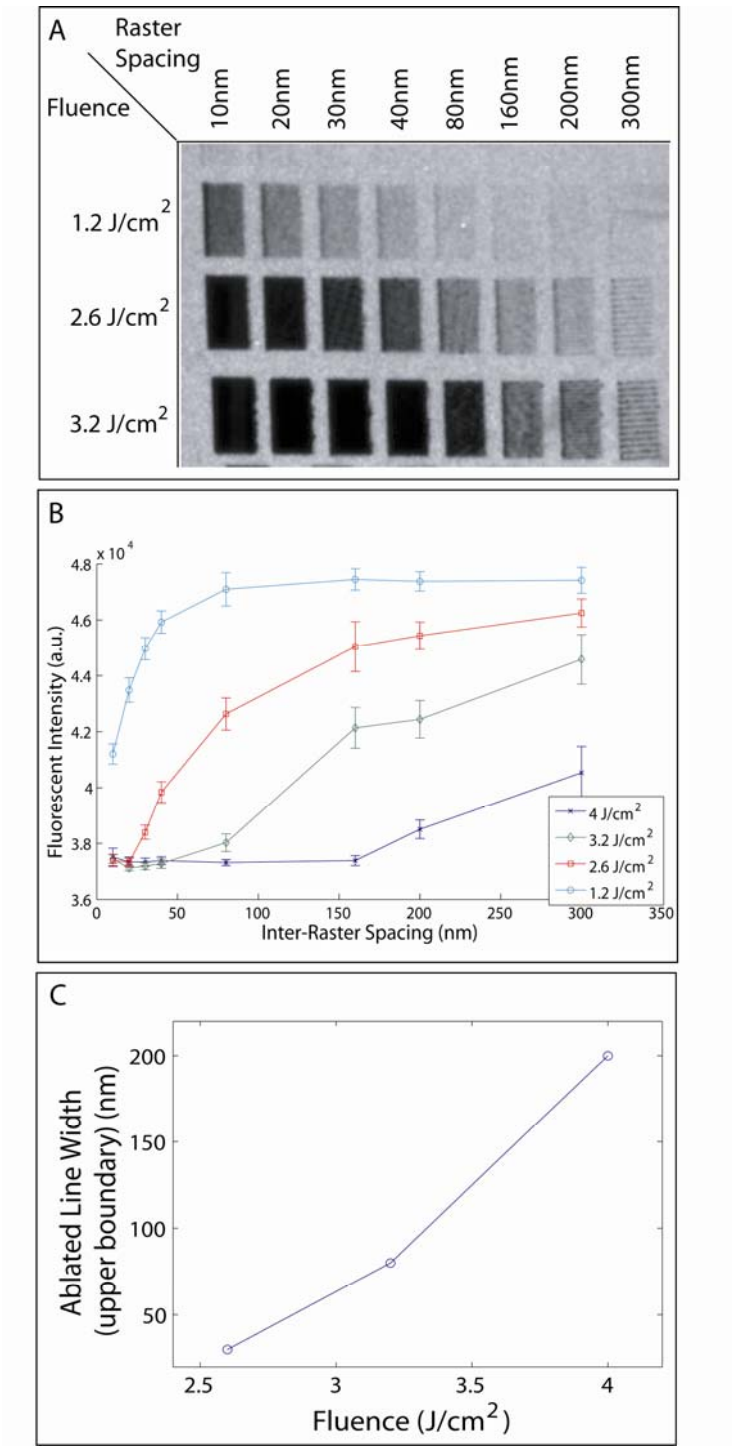

Figure 3-8: Estimate of ablation width by varying raster line spacing. A) Fluorescent micrograph showing the binding of a fluorescent antibody after the surface has been irradiated with varying raster spacing and fluence, damaging the primary antibody previously adsorbed on the surface. B) The fluorescent intensities captured from A. An upper bound for damage width per raster is observed as the closest line spacing for which further spacing does not further decrease fluorescent intensity. C) Plot of upper bound of damage widths derived from panel B.

The AFM data presented in section 4.2, however, seems to imply a deterministic mechanism. The sharp boundaries between the regions where proteins were apparently removed and the regions where the proteins appear unaffected indicate that any damage mechanism remains significantly non-linear.

Once again, a simple geometric explanation may reconcile these two apparently contradictory observations, i.e. very sharp damage boundaries observed via AFM versus a sigmoidal dependence of protein removal/damage on linespacing. At lower fluences there will be less overlap between adjacent laser pulses. At higher fluences, the pulses overlap well, resulting in a linear dependence of fluorescent intensity on linespacing (see Figure 3-7B, fluences of 4J/cm^2 and 3.2 J/cm^2). The damage regions for lower fluences do not overlap as thoroughly. Thus, even if the protein damage or removal is deterministic, resulting in a consistent damage area for each pulse, the sigmoidal relationship observed between fluorescent intensity and line spacing may be expected if the radius of the damage region is small compared to the distance between pulses.

We simulated this hypothesis, considering the portion of a region damaged by rasters composed of an array of damage regions similar to that shown in Figure 3-8B (except we approximated the damage regions from each spot as squares rather than circles for simplicity). We varied the inter-raster spacing, and observed the portion of the total substrate area covered by the damage rasters.

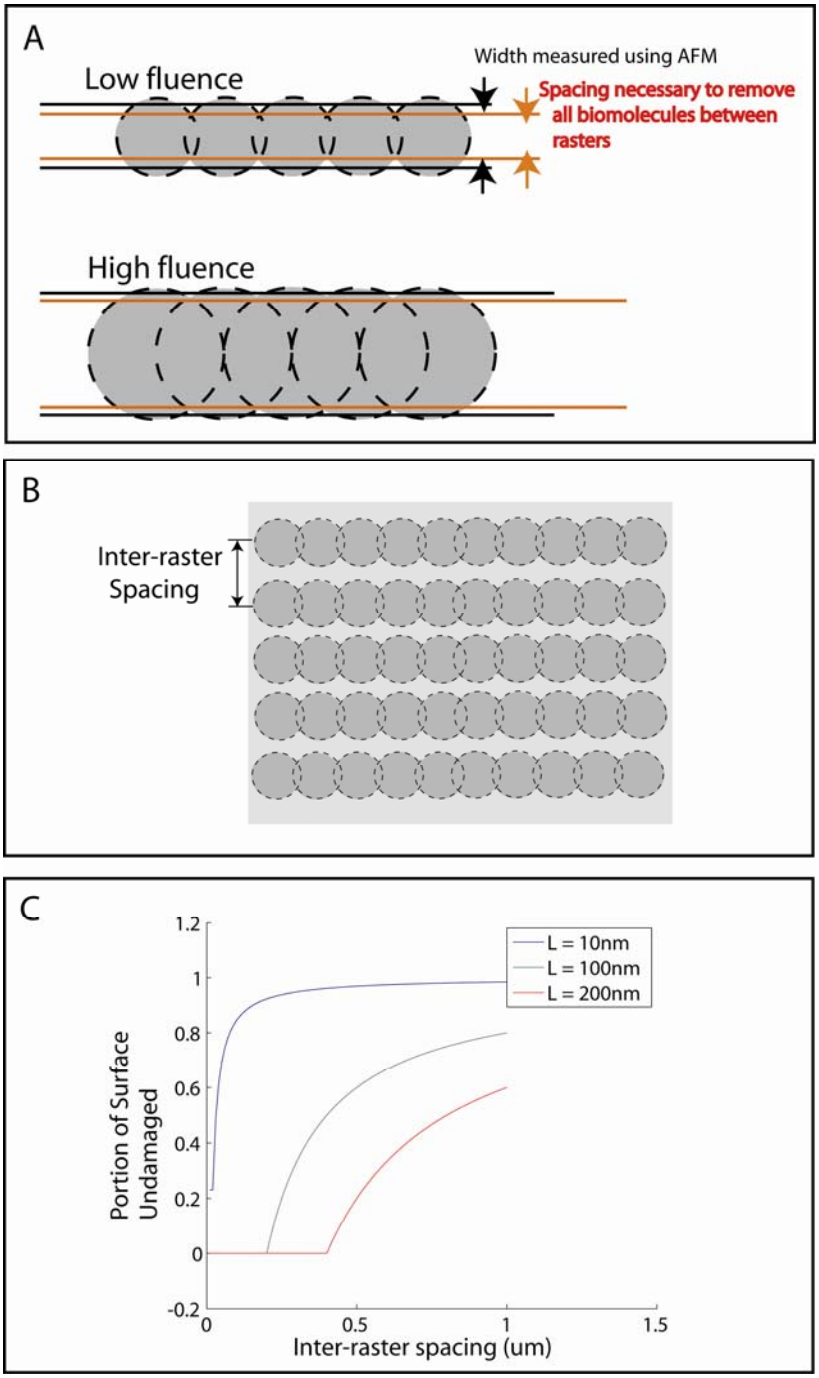

Figure 3-9: Geometric explanation for nonlinear dependence of protein removal on linespacing. A) As the radius of the damage spot becomes small relative to the distance between pulses, the damage raster is no longer approximated well as a rectangular damage swath. Additionally, note that in o. B)The inter-raster spacing necessary to remove all proteins from the surface, notably in the interstices between damage spots, is smaller than the damage width measured using AFM. C) Results of simulations observing the fraction of the substrate damaged as a function of inter-raster spacing. Damage regions resulting from a single pulse is approximated as a square with side length L. These results qualitatively agree well with the observed protein surface densities observed in 3-7B. The dependence is quite non-linear for small damage regions, and becomes approximately linear for larger damage regions.

As shown in Figure 3-9C, the curves of our simulation results are similar to those observed in Figure 3-8B, indicating that this geometric explanation is consistent with our experimental results.

3.5 Demonstration of Nanoscale Residual Feature Width

The preceding sections characterize the width of a protein removal feature. This can be considered "negative" or subtractive patterning, as it is defined primarily by the width of the proteinaceous material removed. However, if the protein removal is sufficiently deterministic and we have sufficient control of the laser position on the substrate, it should be possible to instead leave a narrow feature by irradiating the surrounding region on either side, but leaving a narrow un-irradiated region. We will refer to this small undamaged region as a residual feature.

3.5.1 Methods

3.5.1.1 Flowcell construction and protein adsorption

Flowcells with inlet and outlet were fabricated as described in section 4.3.1. A 50ug/mL solution of biotin-labeled BSA was introduced for 10 minutes before flushing with a 500ug/mL solution of unmodified BSA.

3.5.1.2 Ablation

The laser was rastered across the surface, creating an alternating periodic pattern of “negative” regions where the protein is presumable removed and “positive” lines which are un-irradiated. The laser fluence was 2 J/cm^2, and the inter-raster spacing in the “negative” regions was 20nm. Based on the results of section 4.3, we infer that these parameters result in near-total protein removal in the irradiated regions.

3.5.1.3 Imaging

20ug/mL FITC-streptavidin was loaded for 5 minutes, and then the flowcell was flushed with antifade. The surface was imaged via epifluorescence.

3.5.2 Results

Figure 3-10 illustrates the results of this assay. We find that we are indeed able to generate very narrow feature widths. The line width is estimated by integrating the fluorescent intensity over the patterned region and comparing to the intensity of an unirradiated region:

$$d = \frac{I}{I_{BG}} P ,$$

Where d is the calculated residual line width, I is the average fluorescent intensity in the patterned area, I_{BG} is the average fluorescent intensity of an unablated region, and P is the period of the residual line spacing.

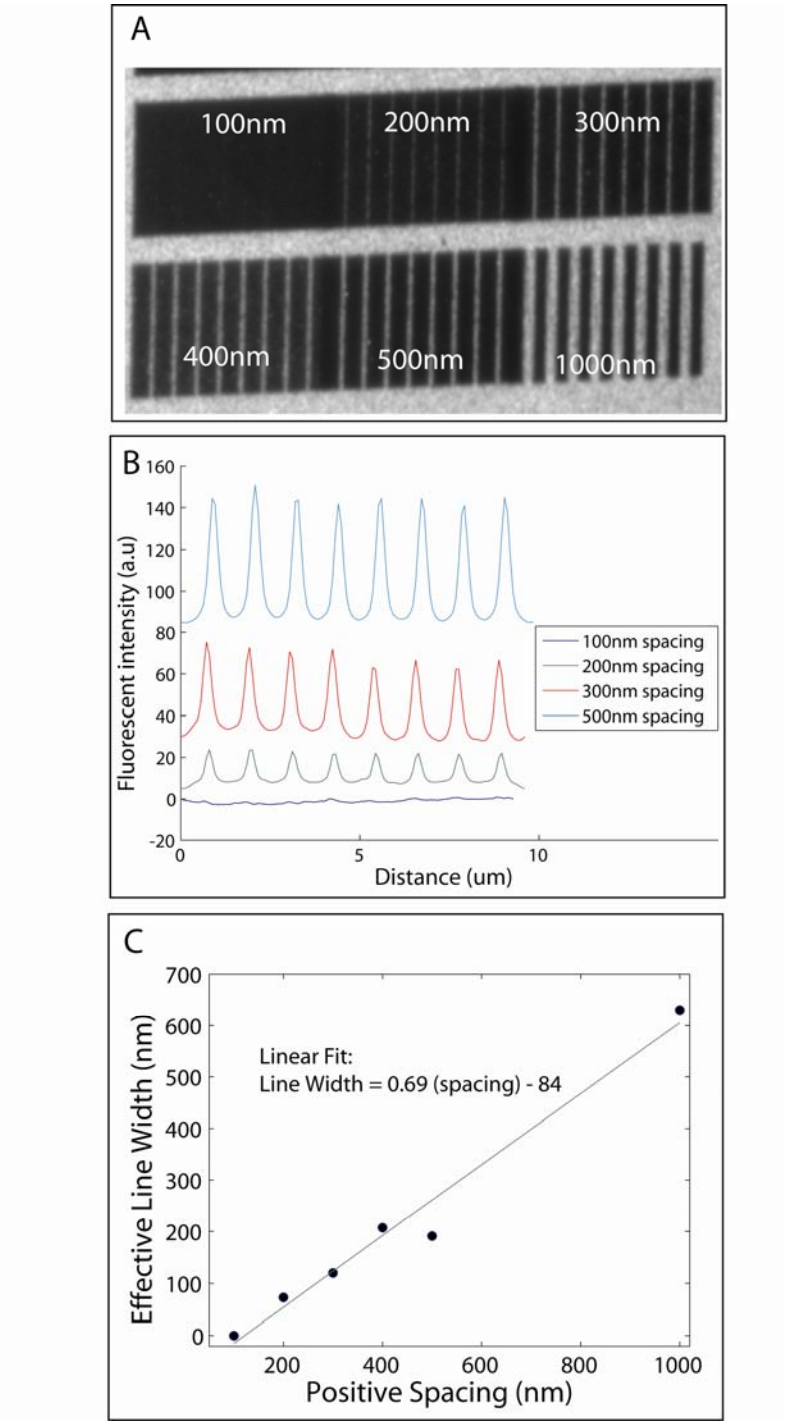

Figure 3-10: Demonstration of residual line patterning. A) Fluorescent micrograph of fluorescently labeled secondary antibody binding to periodic residual lines of previously adsorbed primary antibody after the dark regions have been irradiated. B) Line profiles of fluorescent intensity for various residual line widths. C) Estimated positive line width derived from the fluorescent micrograph in A based on the ratio of average fluorescent intensity in the irradiated region to the intensity of an un-irradiated region.

3.6 Summary

We have demonstrated that proteins can be removed from glass substrates by irradiating the protein-substrate interface with tightly focused ultrafast laser pulses. Notably, we demonstrate that proteins can be removed by this method at intensities significantly below the ablation threshold of glass, enabling the removal of proteins from the surface without damaging the underlying substrate. Ultrafast irradiation below the optical breakdown threshold has been observed and used to damage or remove biomolecules and intracellular structures. However, damage is almost always observed only after multiple pulses. We have demonstrated damage and removal of proteinaceous material in response to single pulses.

Addressing the mechanism by which protein damage and/or removal occurs in our system requires consideration of both how much energy is adsorbed and also how adsorbed energy is partitioned between mechanical effects, thermal effects, or electron excitation[42]. Laser interactions with proteins in aqueous environments are generally safely considered to be dominated by water-laser interaction, as water not only makes up the bulk of the material in the focal region, but the proteins themselves are also highly hydrated. This provides a relatively well-studied system to analyze, though the effects of laser-generated low-density plasmas in water have not received a great deal of attention. Vogel et al. computationally estimated the effects of low-density plasmas in water,

concluding that in addition to chemical damage resulting from free electrons, these low-density plasmas can also cause significant temperature increases and acoustic shock waves at free electron densities as low as $10E^{15}$electrons/cm^3. [35].

Free electrons with energies as low as a few eV have been shown to be capable of fragmenting proteins by damaging their peptide backbone[30]. Extensive fragmentation of proteins would likely cause the majority of fragments to desorb from the surface as the net attraction to the surface decreases. Those that remain adsorbed would be relatively small. This could account for the observation that irradiated regions of a previously protein-coated substrate are lower in height and smoother than un-irradiated regions.

An increase in temperature at the laser focus could possibly lead to thermal protein denaturation. The three-dimensional shape of a protein is maintained by a complex balance of electrostatic forces. If this balance is disrupted, e.g. by changes in the local electrostatic environment, a protein may denature, adopting a non-physiologically active form. A denatured protein may adopt a wide variety of conformations, and it is conceivable that some may experience an overall attraction to an electrically negative surface (e.g. glass) and “flatten” on the surface[43]. This may also explain the significant decrease in height and surface roughness revealed by AFM probing of irradiated regions.

As we'll see in the next chapter, low-density plasmas also have a significant affect on the surface chemistry of glass near the focal volume, and can cause the glass surface to resist protein adsorption. This could lead one to suppose that such a change in adsorptivity of the surface simply causes proteins to desorb, as the electrostatic interaction has been altered. This explanation, however, does not explain the well-defined severance of MTs. As the MTs have significant 3D structure and are significantly stood off from the surface, desorption from the surface does not make sense.

MTs are protein polymers whose structure is maintained by electrostatic interactions. It is possible that the greatly altered electrodynamic environment in the laser-generated low-density plasma could sufficiently disrupt these interactions and lead to localized disassembly of the MT. It is worth noting, however, that the MTs in our assay are significantly more structurally sound and less prone to disassembly than native MTs due to the use of the cross-linker glutaraldehyde to stabilize them. Thus, local disassembly will require disruption of covalent chemical bonds, implying a mechanism beyond a simple alteration of the electrostatic environment. Thermally induced denaturation alone does not explain the severing of cross-linked MTs, and nor do small acoustic shock waves.

Additionally, the ultrafast pulse imposes an intense electric field at the focus, which could impose significant forces on the proteins and their constituent amino

acids, possibly leading to denaturation. It is unclear how much perturbation due to an intense electric field a protein could withstand for such a short period of time and still recover.

Reference List

[1] Du,D., Liu,X., Korn,G., Squier,J., Mourou,G., Laser-Induced Breakdown by Impact Ionization in Sio2 with Pulse Widths from 7 Ns to 150 Fs, Applied Physics Letters, 64 (1994) 3071-3073.

[2] Joglekar,A.P., Liu,H.H., Meyhofer,E., Mourou,G., Hunt,A.J., Optics at critical intensity: Applications to nanomorphing, Proceedings of the National Academy of Sciences of the United States of America, 101 (2004) 5856-5861.

[3] Juhasz,T., Djotyan,G., Loesel,F.H., Kurtz,R.M., Horvath,C., Bille,J.F., Mourou,G., Applications of femtosecond lasers in corneal surgery, Laser Physics, 10 (2000) 495-500.

[4] Maatz,G., Heisterkamp,A., Lubatschowski,H., Barcikowski,S., Fallnich,C., Welling,H., Ertmer,W., Chemical and physical side effects at application of ultrashort laser pulses for intrastromal refractive surgery, Journal of Optics A-Pure and Applied Optics, 2 (2000) 59-64.

[5] Vogel,A., Nonlinear absorption: Intraocular microsurgery and laser lithotripsy, Physics in Medicine and Biology, 42 (1997) 895-912.

[6] Tirlapur,U.K., Konig,K., Cell biology - Targeted transfection by femtosecond laser, Nature, 418 (2002) 290-291.

[7] Zeira,E., Manevitch,A., Khatchatouriants,A., Pappo,O., Hyam,E., Darash-Yahana,M., Tavor,E., Honigman,A., Lewis,A., Galun,E., Femtosecond infrared laser - An efficient and safe in vivo gene delivery system for prolonged expression, Molecular Therapy, 8 (2003) 342-350.

[8] Yanik,M.F., Cinar,H., Cinar,H.N., Gibby,A., Chisholm,A.D., Jin,Y.S., Ben Yakar,A., Nerve regeneration in Caenorhabditis elegans after femtosecond laser axotomy, Ieee Journal of Selected Topics in Quantum Electronics, 12 (2006) 1283-1291.

[9] Konig,K., Riemann,I., Fritzsche,W., Nanodissection of human chromosomes with near-infrared femtosecond laser pulses, Optics Letters, 26 (2001) 819-821.

[10] Watanabe,W., Arakawa,N., Matsunaga,S., Higashi,T., Fukui,K., Isobe,K., Itoh,K., Femtosecond laser disruption of subcellular organelles in a living cell, Optics Express, 12 (2004) 4203-4213.

[11] Sacchi,C.A., Laser-Induced Electric Breakdown in Water, Journal of the Optical Society of America B-Optical Physics, 8 (1991) 337-345.

[12] Williams,F., Varma,S.P., Hillenius,S., Liquid Water As A Lone-Pair Amorphous-Semiconductor, Journal of Chemical Physics, 64 (1976) 1549-1554.

[13] Lenzner,M., Kruger,J., Sartania,S., Cheng,Z., Spielmann,C., Mourou,G., Kautek,W., Krausz,F., Femtosecond optical breakdown in dielectrics, Physical Review Letters, 80 (1998) 4076-4079.

[14] Stuart,B.C., Feit,M.D., Rubenchik,A.M., Shore,B.W., Perry,M.D., Laser-Induced Damage in Dielectrics with Nanosecond to Subpicosecond Pulses, Physical Review Letters, 74 (1995) 2248-2251.

[15] Fan,C.H., Sun,J., Longtin,J.P., Plasma absorption of femtosecond laser pulses in dielectrics, Journal of Heat Transfer-Transactions of the Asme, 124 (2002) 275-283.

[16] Nikogosyan,D.N., Oraevsky,A.A., Rupasov,V.I., 2-Photon Ionization and Dissociation of Liquid Water by Powerful Laser Uv-Radiation, Chemical Physics, 77 (1983) 131-143.

[17] Varel,H., Ashkenasi,D., Rosenfeld,A., Herrmann,R., Noack,F., Campbell,E.E.B., Laser-induced damage in SiO2 and CaF2 with picosecond and femtosecond laser pulses, Applied Physics A-Materials Science & Processing, 62 (1996) 293-294.

[18] Streltsov,A.M., Borrelli,N.F., Study of femtosecond-laser-written waveguides in glasses, Journal of the Optical Society of America B-Optical Physics, 19 (2002) 2496-2504.

[19] Zheng,Y.W., Luk'yanchuk,B.S., Lu,Y.F., Song,W.D., Mai,Z.H., Dry laser cleaning of particles from solid substrates: Experiments and theory, Journal of Applied Physics, 90 (2001) 2135-2142.

[20] Grojo,D., Cros,A., Delaporte,P., Sentis,M., Time-of-flight measurements of ejected particles during dry laser cleaning, Applied Physics B-Lasers and Optics, 84 (2006) 517-521.

[21] Grojo,D., Delaporte,P., Sentis,M., Pakarinen,O.H., Foster,A.S., The so-called dry laser cleaning governed by humidity at the nanometer scale, Applied Physics Letters, 92 (2008).

[22] Cavalleri,A., Sokolowski-Tinten,K., Bialkowski,J., Schreiner,M., der Linde,D., Femtosecond melting and ablation of semiconductors studied with time of flight mass spectroscopy, Journal of Applied Physics, 85 (1999) 3301-3309.

[23] Tran,D.V., Zheng,H.Y., Lam,Y.C., Murukeshan,V.M., Chai,J.C., Hardt,D.E., Femtosecond laser-induced damage morphologies of crystalline silicon by sub-threshold pulses, Optics and Lasers in Engineering, 43 (2005) 977-986.

[24] Tirlapur,U.K., Konig,K., Peuckert,C., Krieg,R., Halbhuber,K.J., Femtosecond near-infrared laser pulses elicit generation of reactive oxygen species in mammalian cells leading to apoptosis-like death, Experimental Cell Research, 263 (2001) 88-97.

[25] Wakida,N.M., Lee,C.S., Botvinick,E.T., Shi,L.Z., Dvornikov,A., Berns,M.W., Laser nanosurgery of single microtubules reveals location-dependent depolymerization rates, Journal of Biomedical Optics, 12 (2007).

[26] Heisterkamp,A., Maxwell,I.Z., Mazur,E., Underwood,J.M., Nickerson,J.A., Kumar,S., Ingber,D.E., Pulse energy dependence of subcellular dissection by femtosecond laser pulses, Optics Express, 13 (2005) 3690-3696.

[27] Peng,C., Palazzo,R.E., Wilke,I., Laser intensity dependence of femtosecond near-infrared optoinjection, Physical Review e, 75 (2007).

[28] Boudaiffa,B., Cloutier,P., Hunting,D., Huels,M.A., Sanche,L., Resonant formation of DNA strand breaks by low-energy (3 to 20 eV) electrons, Science, 287 (2000) 1658-1660.

[29] Swiderek,P., Fundamental processes in radiation damage of DNA, Angewandte Chemie-International Edition, 45 (2006) 4056-4059.

[30] Cloutier,P., Sicard-Roselli,C., Escher,E., Sanche,L., Low-energy (3-24 eV) electron damage to the peptide backbone, Journal of Physical Chemistry B, 111 (2007) 1620-1624.

[31] McConkey,J.W., Malone,C.Y., Johnson,P.V., Winstead,C., Mckoy,V., Kanik,I., Electron impact dissociation of oxygen-containing molecules - A critical review, Physics Reports-Review Section of Physics Letters, 466 (2008) 1-103.

[32] Nolte,S., Momma,C., Jacobs,H., Tunnermann,A., Chichkov,B.N., Wellegehausen,B., Welling,H., Ablation of metals by ultrashort laser pulses, Journal of the Optical Society of America B-Optical Physics, 14 (1997) 2716-2722.

[33] Noack,J., Vogel,A., Laser-induced plasma formation in water at nanosecond to femtosecond time scales: Calculation of thresholds, absorption coefficients, and energy density, Ieee Journal of Quantum Electronics, 35 (1999) 1156-1167.

[34] Kennedy,P.K., A First-Order Model for Computation of Laser-Induced Breakdown Thresholds in Ocular and Aqueous-Media .1. Theory, Ieee Journal of Quantum Electronics, 31 (1995) 2241-2249.

[35] Vogel,A., Noack,J., Mittmann,G., Paltauf,G., Femtosecond-laser-produced low-density plasmas in transparent biological media: A tool for the creation of chemical, thermal and thermomechanical effects below the optical breakdown threshold, Commercial and Biomedical Applications of Ultrafast and Free-Electron Lasers, 4633 (2002) 23-37.

[36] Glezer,E.N., Schaffer,C.B., Nishimura,N., Mazur,E., Minimally disruptive laser-induced breakdown in water, Optics Letters, 22 (1997) 1817-1819.

[37] Schaffer,C.B., Nishimura,N., Glezer,E.N., Kim,A.M.T., Mazur,E., Dynamics of femtosecond laser-induced breakdown in water from femtoseconds to microseconds, Optics Express, 10 (2002) 196-203.

[38] Lodish,H., Berk,A., Zipursky,S.L., Matsudaira,P., Baltimore,D., Darnell,J., Molecular Cell Biology. In 2000, pp. 795-809.

[39] Pampaloni,F., Lattanzi,G., Jonas,A., Surrey,T., Frey,E., Florin,E.L., Thermal fluctuations of grafted microtubules provide evidence of a length-dependent persistence length, Proceedings of the National Academy of Sciences of the United States of America, 103 (2006) 10248-10253.

[40] Lal,R., John,S.A., Biological Applications of Atomic-Force Microscopy, American Journal of Physiology, 266 (1994) C1-&.

[41] Joglekar,A.P., Liu,H., Spooner,G.J., Meyhofer,E., Mourou,G., Hunt,A.J., A study of the deterministic character of optical damage by femtosecond laser pulses and applications to nanomachining, Applied Physics B-Lasers and Optics, 77 (2003) 25-30.

[42] Vogel,A., Noack,J., Nahen,K., Theisen,D., Busch,S., Parlitz,U., Hammer,D.X., Noojin,G.D., Rockwell,B.A., Birngruber,R., Energy balance of optical breakdown in water at nanosecond to femtosecond time scales, Applied Physics B-Lasers and Optics, 68 (1999) 271-280.

[43] Freeman,N.J., Peel,L.L., Swann,M.J., Cross,G.H., Reeves,A., Brand,S., Lu,J.R., Real time, high resolution studies of protein adsorption and structure at the solid-liquid interface using dual polarization interferometry, Journal of Physics-Condensed Matter, 16 (2004) S2493-S2496.

CHAPTER 4

PROTEIN ADSORPTION ON IRRADIATED SURFACES

4.1 Introduction

In the previous chapter, we described the apparent removal of protein from the surface of glass coverslips using femtosecond-pulsed laser irradiation at fluences significantly below the optical breakdown threshold for either glass or water. In this chapter we will continue to probe the interaction of ultrafast laser irradiation at the glass-water and glass-proteinaceous solution interfaces. We examine the adsorptivity of representative target proteins on both un-coated and previously protein-coated glass surfaces which have been irradiated using ultrafast laser pulses. As we develop a picture of the mechanism responsible for the observed changes in adsorptivity, we are also led to greater insights into the mechanism of protein removal described in the Chapter 3.

As discussed in earlier chapters, the ability to selectively alter the adsorptivity of surfaces enables development of various biodevices and basic research. In this chapter, we examine another method of manipulating surfaces with nanoscale

precision to influence the deposition of proteins using non-destructive ultrafast laser irradiation.

In this method, a surface is irradiated with relatively low intensity laser pulses, at or significantly below the optical breakdown threshold of glass or water. This results in a long-term change in surface charge on glass, which in turn alters the protein adsorptivity of the irradiated surfaces. We will briefly discuss possible mechanisms underlying this change in surface charge, focusing on the generation of low density plasmas in the focal volume and the resulting chemical and thermal effects.

4.2 Protein Adsorption on irradiated uncoated glass surfaces

We begin this study by simply irradiating a surface with varied fluence and observing the degree of adsorption of a model protein, neutravidin, to the irradiated surface. Neutravidin is a globular protein with four high affinity binding sites for biotin, making it a useful biomolecular “glue” which could be used in subsequent applications to bind a wide variety of biotinylated proteins of other biomolecules.

4.2.1 Materials and Methods

4.2.1.1 Preparation of Substrates:

Glass coverslips were rinsed with isopropanol and DI water and blown dry with nitrogen. They were then secured using double-sided sticky tape to a conventional glass microscope slide incorporating an inlet and outlet as described in section 4.3.1.

4.2.1.2 Surface Irradiation

The flowcell was loaded with PBS and mounted on a piezo-driven nanostage on an inverted microscope. For each tested fluence, the laser was rastered across a series of rectangular regions on the surface of the coverslip, with the laser focus at the liquid-glass interface. Pulse energy was controlled using a set of neutral density filters. The velocity of the stage movement and the spacing between rasters was chosen such that the distance between individual laser pulses is approximately the radius of the spot size.

4.2.1.3 Target protein adsorption

After irradiation, 20ug/mL neutravidin in PBS at pH = 7.1 was loaded into the flowcell, and allowed 15 minutes to interact. The flowcell was then flushed sequentially with PBS and antifade.

4.2.1.4 Imaging and data acquisition

Irradiated regions were imaged under epi-fluorescence and intensity values were measured for each ablated region and recorded using a custom MatLab script.

4.2.2 Results

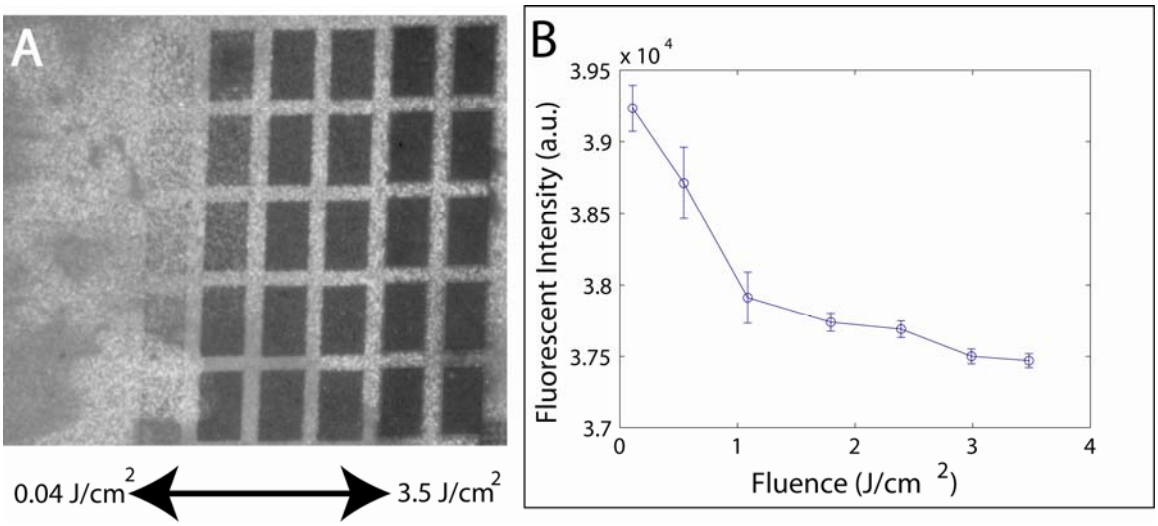

Figure 4-1: Adsorption of neutravidin to irradiated glass surface. A) Fluorescent micrograph of fluorescently labeled neutravidin adsorbed to glass surface after laser irradiation. B) The amount of neutravidin adsorbed is monotonically dependent on the intensity the surface is irradiated with. Note that at fluence of 0.04 J/cm2, the amount of protein adsorbed is not significantly different from the amount adsorbed to un-irradiated regions.

As can be seen in Figure 4-1, irradiation of the glass surface results in decreased neutravidin adsorption. The surface density of neutravidin decreases monotonically with increased fluence.. This implies that there has been a change in the glass surface which affects its adsorptivity. We have performed this assay

with an extended length of time, up to 24 hours, after irradiation before introducing the fluorescent protein. These assays showed similar results, with protein adsorption severely attenuated with increasing fluence.

Protein adsorption on surfaces is primarily an electrostatic effect. This leads us to hypothesize that the surface charge of the irradiated glass has been altered by exposure to the low intensity laser pulse. We test this hypothesis in the following section.

4.3 Interaction of Charged Molecules with Irradiated Glass Surface

4.3.1 Motivation

We hypothesize that the source for the difference in adsorptivity between irradiated and un-irradiated glass surfaces lies in a change in the surface potential of the glass caused by laser irradiation. More specifically, we hypothesize that irradiated surfaces exhibit a lower (less negative) potential as compared to an un-irradiated surface due to a reduction of the density of silanol groups on the surface. An obvious consequence of this hypothesis is that positively charged particles will exhibit weaker interactions with irradiated regions than un-irradiated regions.

In order to test this hypothesis, we introduced a positively charged fluorophore, rhodamine B, to a glass surface which had been irradiated at varied fluence and observed its adsorption.

4.3.2 Methods

Coverslips were cleaned, flowcells fabricated, and coverslip surface irradiated as described in section 5.2.1 above. 3ug/mL rhodamine B in DI water was added to the flowcell and epi-fluorescent images were taken.

4.3.3 Results

As shown in Figure 4-2, rhodamine B adsorption does decrease monotonically, with increased fluence possibly with a decreasing monoexponential dependence on fluence. This supports our hypothesis that the resistance to protein adsorption seen in irradiated surfaces in section 5.2 is caused by a decrease in the surface charge of the irradiated glass surface.

From this result, we can estimate the relationship of surface charge to incident fluence. At equilibrium, the proportion of fluorophore bound to the surface should follow a Boltzmann distribution.

$$I(f) \propto \frac{p_{adsorb}}{p_{solution}} = e^{\Delta E / kT}$$

Where I(f) is the fluorescent intensity, which is proportional to the amount of fluorophore on the surface, p_{adsorb} is the probability of a fluorophore binding to the

surface, $p_{solution}$ is the probability of a fluorophore remaining in solution, k is the Boltzmann constant, T is the temperature, and ΔE is the change in energy associated with the binding of a fluorophore. To a first approximation, it is reasonable to assume that this binding energy associated with the electrostatic interaction between the charged fluorophore particle and a charged surface is proportional to the charge of the surface.

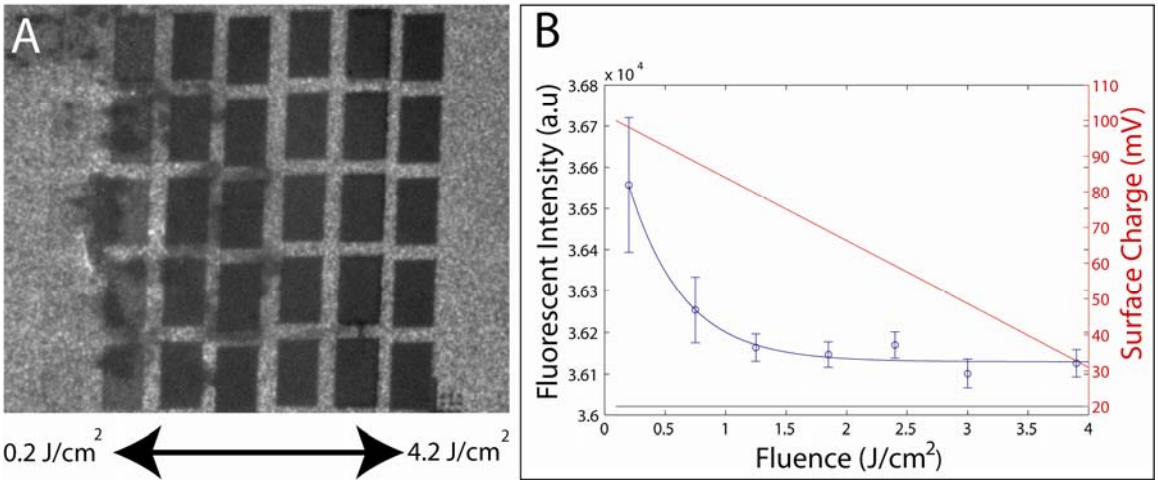

Figure 4-2: Adsorption of rhodamine B to irradiated glass surface. A) Fluorescent micrograph of the charged fluorophore rhodamine B adsorbed to glass surface after laser irradiation. B) The amount of rhodamine B adsorbed is monotonically dependent on the intensity the surface is irradiated with. Based on this interaction, the surface charge of the irradiated glass surface is estimated, demonstrated on the right y-axis.

By relating a decreasing monoexpenential fit of I(f) to the expression for I(f) described above by the Boltzmann distribution above, we can make an estimated prediction of the charge of the surface as a function of fluence, Φ(f). This yields a simple linear relationship between fluence and surface charge, Φ(f)=Af+B.

Noting that the surface charge of unmodified glass in DI water is 100mV, and that the surface charge of glass ablated near the ablation threshold has been estimated by electroosmotic mobility of charged fluorophores to be 31mV, we can solve for A and B, yielding $\Phi(f)=100mV-17.25cm^2 \cdot mV \cdot J^{-1} * f$. Figure 4-2B shows a fit of a decreasing mono-exponential to our observed fluorescent values, and, on the right axis, the estimated surface charge based on the above analysis..

This alteration of surface charge of the glass surface resulting from laser irradiation is likely explained by a change in the surface chemistry of the glass surface. The silica surface is predominantly composed of siloxane bridges and silanol groups (see Figure 4-3). Silanol groups are relatively reactive and more highly charged, while siloxane bridges tend to be quite inert and less charged[1].

It is well-characterized that heating silica causes silanol groups to dehydroxylate, condensing to siloxane bridges[1;2]. This results in a surface which is less reactive and more hydrophobic. This condensation begins to occur at temperatures around 170C, and near-complete dehydroxylation of the surface requires temperatures near 1000C to be maintained for several hours[1].

It is possible that in our experiments, the focal region reaches temperatures sufficient to drive silanol dehydroxylation. This temperature dissipates very quickly, however, making it unlikely that temperature increase alone drives

dehydroxylation of the surface. It is also possible the photon absorption drives the dehydroxylation more directly. The OH bond dissociation energy is 4.43eV[3]. It is possible that this bond could be severed by a 2-photon absorbance, which could subsequently enable the condensation reaction to spontaneous complete. This photochemical explanation seems more plausible, considering the timescale necessary for thermal dehydroxylation[3].

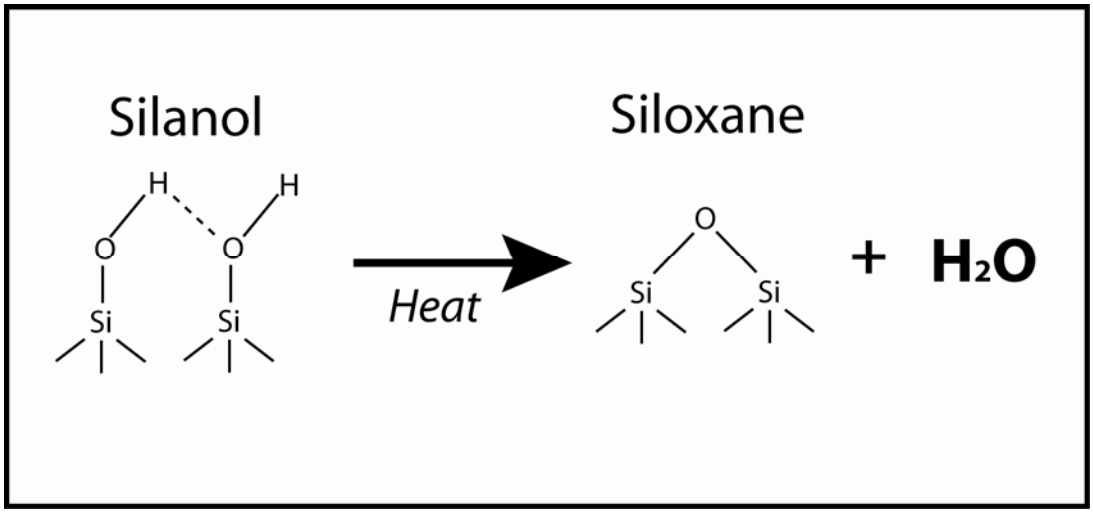

Figure 4-3: Silica dehydroxylation. With the imposition of heat, silanol groups are condensed to form siloxane bridges, resulting in a silica surface which is less reactive, less charged, and more hydrophobic.

4.4 Adsorption on irradiated protein-coated surfaces

4.4.1 Motivation

In chapter 3, we demonstrated that proteins could be removed from a glass surface with ultrafast pulses of fluence considerably below the breakdown threshold of water or glass. We observed a smoothing and decrease in phase

response of the AFM signal in irradiated regions of a previously protein-coated glass substrate. Above, we also observed that there is a change in the glass surface chemistry after irradiation with low intensity pulses. We are led to consider whether proteins are fully removed from the surface, as one is likely to naively suppose from the protein removal results of section 3.3. In this section, we observe adsorption to surfaces which were protein-coated prior to irradiation in order to test the hypothesis that protein is removed cleanly from the surface. To do so, we irradiate a protein-coated surface, and observed the adsorbtivity of the resulting surface for the same protein introduced a second time.

4.4.2 Methods

Single pass surface irradiation: The glass surface was cleaned and constructed in a flowcell as described in section 4.2.2. Prior to irradiation, a 50ug/mL Alexa-488 goat anti-rabbit IgG antibody in a 20-fold dilution of PBS in DI water was introducted for 15 minutes before flushing with PBS. The protein was suspended in a diluted PBS solution to decrease ionic strength and thereby strengthen adsorption. Square regions at the coverslip surface were again irradiated with varying pulse energies as described in 5.2.2. After irradiation, the same protein solution was again introduced for 15 minutes before flushing the flowcell with antifade and imaging.

Multiple pass surface irradiation: This series of experiments was performed as the "single pass" described above, except each irradiated region underwent multiple exposures of irradiation before the second protein adsorption, with the number of exposures varied from 1 to 10.

4.4.3 Results

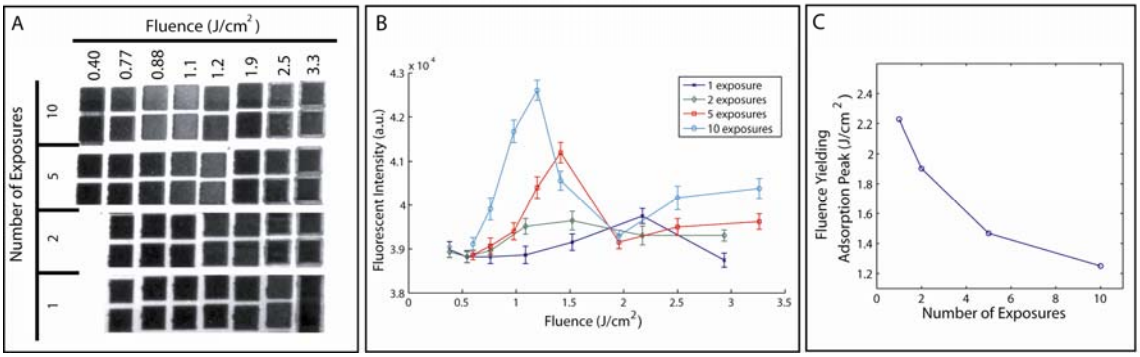

Figure 4-4: Adsorption to irradiated protein-coated surfaces after multiple irradiation exposures. A) Fluorescence micrograph of a series of protein-coated regions which have been irradiated with varying fluence, with varying number of exposures, before re-introduction of a fluorescent protein. Contrast of the image has been enhanced to better illustrate re-adsorption in the irradiated areas. B) Fluorescent intensity reported by re-adsorbed protein in the irradiated regions. Note that higher number of exposures appears to result in a larger peak adsorption density. Also note that the fluence at which the peak occurs varies with the number of exposures. C) The fluence at which the peak adsorption occurs is dependent on the number of exposures.

We find that a surface irradiated in this way exhibits adsorbtive behavior markedly different from surfaces which were not coated with protein prior to irradiation. The results indicate that the protein first adsorbed is not in fact removed completely or cleanly, but rather leaves a residue that affects the adsorptivity of the surface.

This experiment yields a number of interesting observations. First, the adsorptivity of surfaces which were protein-coated prior to irradiation exhibit markedly different adsorbtive behavior as compared to surfaces which were un-coated prior to irradiation. On irradiated un-coated surfaces, adsorbtivity appears to decrease monotonically, approximately exponentially, from a maximum near the background value (the value of the un-irradiated regions) at low fluence to near zero at the glass breakdown threshold. When the surface had been coated with antibody prior to irradiation, however, the adsorption profile was not exponential or even monotonic. Instead, a peak adsorption was observed for surface irradiated at 2.2 J/cm^2. Note that this peak adsorption was still considerably lower than the adsorption in unirradiated regions.

This behavior is curious. To further examine this effect, we exposed regions multiple times, each region irradiated multiple times at the same fluence. In varying the number of exposures from one to ten, we found that in all cases, the adsorption profile after re-adsorption of the antibody exhibited a peak. Interestingly, the fluence at which the peak adsorptivity was observed and the magnitude of the peak adsorptivity shifted significantly with varied number of exposures.

This may indicate competing mechanisms. We have noted that the surface charge of the surface appears to decrease with increased fluence, resisting protein adsorption. We have also noted that for relatively high fluence, proteins

appear to be removed from the surface. Perhaps, when a protein-coated surface is irradiated with relatively low fluence, a probabilistic mechanism damages the proteins on the surface, altering the charge they present to subsequently adsorbed proteins. At some level of damage, they tend to resist adsorption the least, resulting in a peak of adsorption. It is unclear what kind of damage mechanism would result in this behavior.

4.5 Serial adsorption

4.5.1 Motivation

The previous section indicates that for some fluences, protein-coated surfaces for which are irradiated exhibit a relative peak in adsorption of subsequently introduced proteins. With this observation, we suppose that it is possible to serially pattern a multitude of different varieties of protein by iteratively irradiating different regions and adsorbing different varieties of protein. This section illustrates our attempt to do so, serially adsorbing a series of proteins tagged with different fluorophores.

4.5.2 Methods

Coverslips were cleaned and flowcells fabricated as described in section 5.2.1 above. 200ug/mL avidin was introduced to the flowcell for 10 minutes before flushing with PBS. A series of regions were then irradiated with varying fluence

as in section 5.2. 10ug/mL FITC-labeled streptavidin was then introduced for 5 minutes and flushed with PBS. A second series of regions was irradiated before introducing Cy3-labeled streptavidin for 5 minutes and flushing with PBS. A third series of regions was irradiated, followed by introduction of Alexa350-labeled streptavidin for 5 minutes and a final flush with antifade. Epifluorescent images were taken in the three respective fluorescent channels.

4.5.3 Results

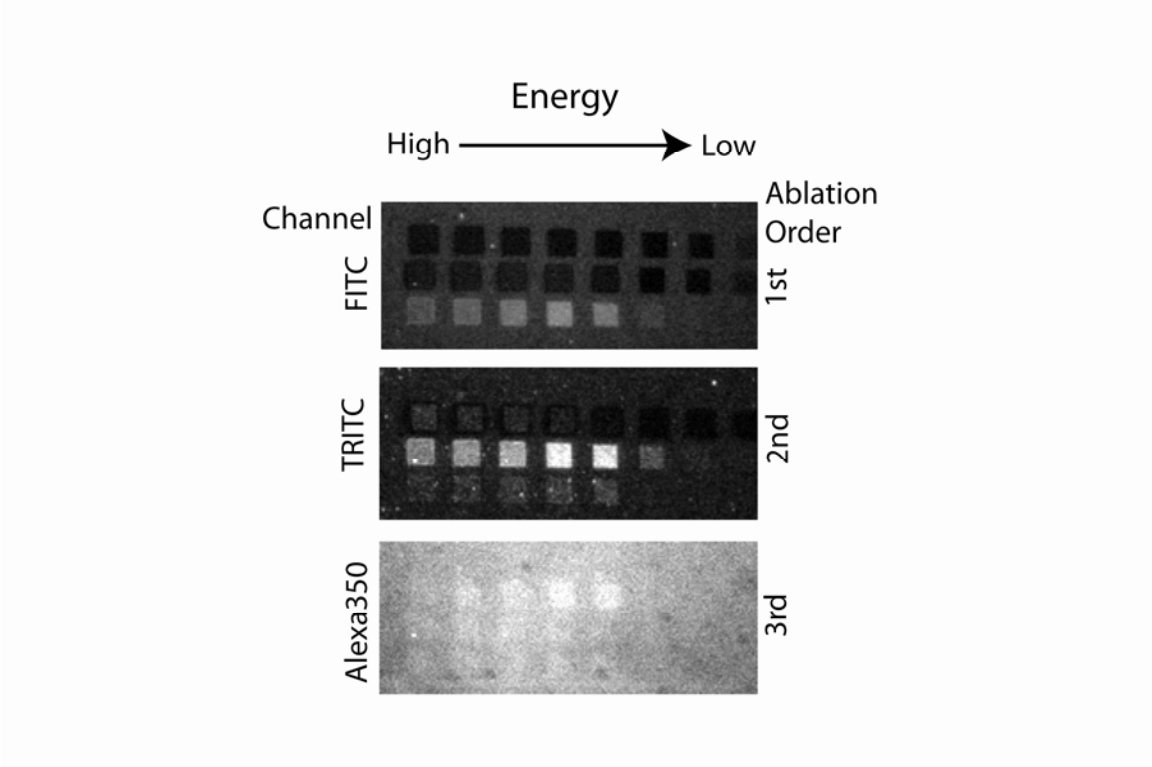

Figure 4-5: Serial patterning of three streptavidin moities. Streptavin tagged with three different fluorophores have been segregated in different regions. Each variety of labeled-streptavidin was introduced after a series of patches were irradiated with varied fluence. Note that each variety of labeled streptavidin is localized to the one row which was irradiated immediately prior to introduction of that each respective protein, and that the peak adsorption consistently occurs at a fluence of approximately 2J/cm^2.

We find that we are successfully able to segregate the adsorption of the three moieties of streptavidin. In each case, we again see a peak in the adsorptivity profile for each type of labeled streptavidin, and that peak occurs at the same fluence for each variety of streptavidin, and thus occurs at the same fluence for each adsorption cycle. This method provides a possible method of producing high resolution patterns of multiple proteins. Streptavidin binds very strongly to biotin, and the biotinylation of proteins is a very common and generally straight-forward functionalization. Streptavidin thus provides an attractive base layer on which to build an stack of one's choice of proteins.

4.6 Summary

We have shown that irradiation of glass surfaces results in a relatively long-lived change in its surface properties, affecting, in particular, the propensities of proteins to adsorb. By observing the interaction of a charged fluorophore with irradiated surfaces, we have identified a change in the surface charge as a dominant factor in this change of surface properties. We attribute this change to a laser-induced decrease in the density of silanol groups on the glass surface. This change does not seem to be a result of thermal effects, as thermal dehydroxylation of glass takes place on time scales of hours, many orders of magnitude longer than the time the glass is heated by our femtosecond pulses. in section 5.4, then, must proceed by a different mechanism.

In considering the impact of the results of our inquiry into protein adsorption on irradiated surfaces, we should note that any mechanism that relies on a change in electrostatic surface charge to affect adsorption is likely to have a wide range of behaviors, depending on the protein of interest and buffer conditions. As proteins are an extremely heterogenous group, with widely varying surface charges and hydrophobicities, the adsorption of different proteins will be affected differently by changes in charge of the surface. The complicated 3-dimensional structure of proteins and their ability to expose different charged functional groups depending on their folding state further complicates predictions of adsorption behavior. Thus it is difficult to predict the response of any particular protein to a change in surface charge such as the one we have imposed. The value in these studies is likely to lie more in aiding a basic understanding of interactions of ultrafast irradiation with glass and biological media than in derivation of a predictive model of adsorption on irradiated surfaces.

Reference List

[1] Iler,R.K., The chemistry of silica, Wiley, New York, 1979.

[2] Vogel,W., Glass chemistry, Springer-Verlag, New York, 1994.

[3] Halfpenny,D.R., Kane,D.M., Lamb,R.N., Gong,B., Surface modification of silica with ultraviolet laser radiation, Applied Physics A-Materials Science & Processing, 71 (2000) 147-151.

CHAPTER 5

GUIDANCE OF MOTILE FIBROBLASTS BY SELECTIVE IRRADIANCE OF FIBRONECTIN

5.1 Introduction

One important application of protein patterning is the control of cellular behavior on patterned substrates by engineering the presentation of adhesion-promoting or other signaling proteins on the surface. Cellular behaviors such as differentiation, migration, or apoptosis are influenced heavily by interactions with extracellular signal proteins[1]. The cellular response may be influenced by the average density of signal proteins, their spatial distribution, and conformation[2-7]. Studies aimed at probing these spatial influences not only lend insight into basic mechanisms of cellular responses, but also have practical applications, perhaps most notably in the development and optimization of bioactive scaffolds for tissue engineering applications[8;9].

Many techniques have been used to control the distribution of biomolecules for the purpose of studying the effect on cellular behavior. Many of these techniques are described in Chapter 1, and have been recently reviewed elsewhere[10-12].

Control of cell placement and behavior also allows fabrication of cell-based biosensors. These cell-based biosensors may be used to detect the presence of a toxin or pathogen in the environment based on the cellular response[12-14], or to screen the pharmacologic response of cells mimicking in vivo behavior in drug discovery assays[15;16].

In this chapter, we describe the guidance of motile fibroblasts by modifying the presentation of surface-immobilized proteins using the laser-based protein removal technique discussed in chapter 3. Fibroblasts are motile cell types which play a critical role in wound healing, producing a number of extracellular matrix components to repair damaged connective tissues, including collagen, elastin, and glycosaminoglycans[17]. In particular, we use the 3T3 fibroblast cell line, a line which was derived from primary mouse embryonic fibroblasts[18] which is easily maintained and exhibits robust motility in culture. Fibroblasts, like many motile cell types, migrate preferentially on surfaces presenting the adhesion-promoting protein fibronectin[19]. By selectively removing fibronectin from the cells' path using laser irradiation, we direct their movement onto un-irradiated regions.

The guidance of motile cells by presenting the cell with a surface selectively coated with an adhesion-promoting protein such as fibronectin has been demonstrated by a variety of patterning techniques[6;20;21]. However, our method provides a general method to modify the cellular microenvironment in

situ, and thereby presents itself as a useful tool for study of cellular response to changes in extracellular environment imposed during observation.

5.2 Methods

5.2.1 Culture Dish Functionalization

Glass-bottom cell culture dishes were coated with fibronectin by adding to 20ug/mL fibronectin for 30 minutes[22]. The dish was then rinsed thrice with PBS before adding non-CO2 buffered media (8% calf serum, in L-15 media with 4.5 g/L glucose).

5.2.2 Cell Culture

3T3 fibroblast cell cultures were maintained by incubating at 37C in 10% CO2 in DMEM with 8% calf serum and 4.5g/L glucose. Approximately 2 hours prior to surface patterning, cells were transferred to the non-CO2 buffered media above and seeded at approximately 1E4 cells/cm^2 on fibronectin-coated glass-bottom culture dishes coated.

5.2.3 Protein Removal by Laser Irradiation

A glass-bottomed cell culture dish which has been seeded with fibroblasts was placed on a piezo-driven nanostage on a Zeiss inverted microscope. The laser was focused through a 40x, 0.65NA objective. Portions of the surface around a motile cell were irradiated with a fluence of 2.1J/cm^2 such that the cell would

encounter a surface which had been irradiated. The cell was then observed under phase contrast for up to 24 hours, with images taken at a rate of one per minute.

5.3 Results

Cell behavior upon encountering the irradiated region varied. Interactions of fifteen cells motile cells with irradiated boundaries were observed. Most cells (12 interactions out of the 15 total observed) diverted the direction of their movement, avoiding the irradiated region. Other cells temporarily ceased movement upon encountering the irradiated region before adopting an elongated form and eventually resuming movement after the elongated pseudopod reached beyond the irradiated region (3 interactions out of 15 total). A small portion of cells continued movement across the irradiated region without a significant change in direction or cell shape (2 interactions out of 15 total). Both of these cells had recently undergone mitosis, after which the two daughter cells appear to move very rapidly away from each other.

Figure 5-1 shows a typical result when a motile cell was “enclosed” by an irradiated border. The cell follows a circular path along the edge of the irradiated region for many hours before finally adopting an elongated form and reaching beyond the irradiated border and moving out of the irradiated region.

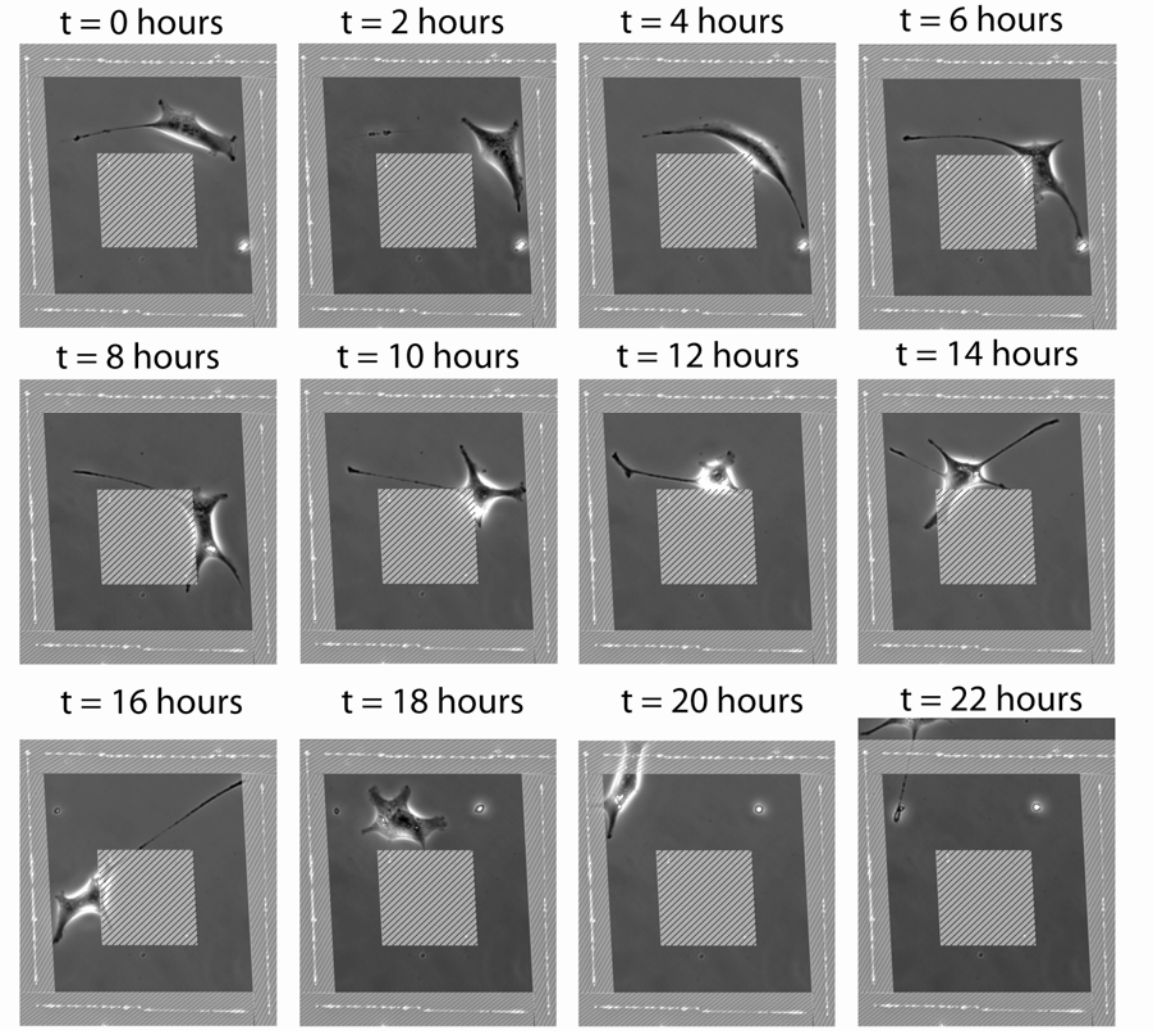

Figure 5-1: Confinement of a fibroblast by irradiation of surrounding surface. The lightened, hashed area represents the region of the surface which was irradiated. The cell's movement was confined inside the irradiated boundary for approximately a day.

5.4 Discussion

This experiment demonstrates that we are indeed able to guide cell movement by laser irradiation, showing that we have successfully modified the

microenvironment of the cell in situ. We gathered sufficient data to describe successful guidance, but we did not gather enough data to yield detailed statistics on the prevalence of the different behaviors noted. It would be interesting to observe the width of the irradiated area necessary to alter the motile cells' path, the density of irradiation necessary to alter the path, and the likelihood of adopting the elongated cell shape noted above. This could be correlated to time spent interacting with the irradiated form (i.e. the probability of adopting this shape could increase with increased exposure time), or could simply be probabilistic (a constant probability per some interaction time).

The significance of these experiments lies less in the knowledge gained about fibroblast motility, however, than in the demonstration of modification of the cells' surroundings in situ. Typically, an experiment such as this would be performed by immobilizing the biomolecule of choice on a substrate in a predesigned pattern before introducing cells, and then searching to find cells interacting with the pattern in the desired orientation, exhibiting the desired behavior, etc. For many assays, this is adequate. It would facilitate many assays, however, if one could instead find a cell of interest first, and then introduce an **arbitrary** pattern near it **on-the-fly**. This is the type of flexibility that our technique allows.

Though we demonstrate this on a 2-dimensional glass substrate, the technique is plausibly extensible to modification of the 3-dimensional micro-environment, selectively removing or damaging biomolecules on 3-dimensional scaffolds. This

extensibility would make it possible to study cells in a situation much closer to their native environment. In the body, cells interact with a complex 3-dimensional environment. It has become clear that cells behave differently when artificially confined to a 2D surface, as is the norm in studying cell cultures, than they do in their native environment. Studying cells in an environment closer to their native environment is likely to yield more accurate observations of cellular behavior, which is useful not only in developing basic biological understanding, but is also crucial in developing biomaterials for tissue engineering applications which promote cell infiltration and proper tissue organization[8].

Reference List

[1] Bourdoulous,S., Orend,G., MacKenna,D.A., Pasqualini,R., Ruoslahti,E., Fibronectin matrix regulates activation of Rho and Cdc42 GTPases and cell cycle progression, Journal of Cell Biology, 143 (1998) 267-276.

[2] Lehnert,D., Wehrle-Haller,B., David,C., Weiland,U., Ballestrem,C., Imhof,B.A., Bastmeyer,M., Cell behaviour on micropatterned substrata: limits of extracellular matrix geometry for spreading and adhesion, Journal of Cell Science, 117 (2004) 41-52.

[3] Craighead,H.G., Turner,S.W., Davis,R.C., James,C., Perez,A.M., St.John,P.M., Isaacson,M.S., Kam,L., Shain,W., Turner,J.N., Banker,G., Chemical and Topographical Surface Modification for Control of Central Nervous System Cell Adhesion, Biomedical Microdevices, 1 (1998) 49-63.

[4] Jiang,X.Y., Bruzewicz,D.A., Wong,A.P., Piel,M., Whitesides,G.M., Directing cell migration with asymmetric micropatterns, Proceedings of the National Academy of Sciences of the United States of America, 102 (2005) 975-978.

[5] Dike,L.E., Chen,C.S., Mrksich,M., Tien,J., Whitesides,G.M., Ingber,D.E., Geometric control of switching between growth, apoptosis, and differentiation during angiogenesis using micropatterned substrates, In Vitro Cellular & Developmental Biology-Animal, 35 (1999) 441-448.

[6] Chen,C.S., Mrksich,M., Huang,S., Whitesides,G.M., Ingber,D.E., Geometric control of cell life and death, Science, 276 (1997) 1425-1428.

[7] Chen,C.S., Tan,J., Tien,J., Mechanotransduction at cell-matrix and cell-cell contacts, Annual Review of Biomedical Engineering, 6 (2004) 275-302.

[8] Griffith,L.G., Naughton,G., Tissue engineering - Current challenges and expanding opportunities, Science, 295 (2002) 1009-+.

[9] Lee,S.H., Moon,J.J., West,J.L., Three-dimensional micropatterning of bioactive hydrogels via two-photon laser scanning photolithography for guided 3D cell migration, Biomaterials, 29 (2008) 2962-2968.

[10] Falconnet,D., Csucs,G., Grandin,H.M., Textor,M., Surface engineering approaches to micropattern surfaces for cell-based assays, Biomaterials, 27 (2006) 3044-3063.

[11] Folch,A., Toner,M., Microengineering of cellular interactions, Annual Review of Biomedical Engineering, 2 (2000) 227-+.

[12] Jung,D.R., Kapur,R., Adams,T., Giuliano,K.A., Mrksich,M., Craighead,H.G., Taylor,D.L., Topographical and physicochemical modification of material surface to enable patterning of living cells, Critical Reviews in Biotechnology, 21 (2001) 111-154.

[13] Park,T.H., Shuler,M.L., Integration of cell culture and microfabrication technology, Biotechnology Progress, 19 (2003) 243-253.

[14] Ziegler,C., Cell-based biosensors, Fresenius Journal of Analytical Chemistry, 366 (2000) 552-559.

[15] Bhadriraju,K., Chen,C.S., Engineering cellular microenvironments to cell-based drug testing improve, Drug Discovery Today, 7 (2002) 612-620.

[16] Schwenk,J.M., Stoll,D., Templin,M.F., Joos,T.O., Cell microarrays: An emergmg technology for the characterization of antibodies, Biotechniques, (2002) 54-+.

[17] Lodish,H., Berk,A., Zipursky,S.L., Matsudaira,P., Baltimore,D., Darnell,J., Molecular Cell Biology. In 2000, pp. 795-809.

[18] Todaro,G.J., Green,H., Quantitative Studies of Growth of Mouse Embryo Cells in Culture and Their Development Into Established Lines, Journal of Cell Biology, 17 (1963) 299-&.

[19] Postlethwaite,A.E., Keskioja,J., Balian,G., Kang,A.H., Induction of Fibroblast Chemotaxis by Fibronectin - Localization of the Chemotactic Region to A 140,000-Molecular Weight Non-Gelatin-Binding Fragment, Journal of Experimental Medicine, 153 (1981) 494-499.

[20] Kandere-Grzybowska,K., Campbell,C.J., Mahmud,G., Komarova,Y., Soh,S., Grzybowski,B.A., Cell motility on micropatterned treadmills and tracks, Soft Matter, 3 (2007) 672-679.

[21] Singhvi,R., Kumar,A., Lopez,G.P., Stephanopoulos,G.N., Wang,D.I.C., Whitesides,G.M., Ingber,D.E., Engineering Cell-Shape and Function, Science, 264 (1994) 696-698.

[22] Tzoneva,R., Faucheux,N., Groth,T., Wettability of substrata controls cell-substrate and cell-cell adhesions, Biochimica et Biophysica Acta-General Subjects, 1770 (2007) 1538-1547.

[23] Hahn,M.S., Taite,L.J., Moon,J.J., Rowland,M.C., Ruffino,K.A., West,J.L., Photolithographic patterning of polyethylene glycol hydrogels, Biomaterials, 27 (2006) 2519-2524.

[24] Kaehr,B., Allen,R., Javier,D.J., Currie,J., Shear,J.B., Guiding neuronal development with in situ microfabrication, Proceedings of the National Academy of Sciences of the United States of America, 101 (2004) 16104-16108.

[25] Wosnick,J.H., Shoichet,M.S., Three-dimensional chemical Patterning of transparent hydrogels, Chemistry of Materials, 20 (2008) 55-60.

[26] Luo,Y., Shoichet,M.S., A photolabile hydrogel for guided three-dimensional cell growth and migration, Nature Materials, 3 (2004) 249-253.

[27] Hern,D.L., Hubbell,J.A., Incorporation of adhesion peptides into nonadhesive hydrogels useful for tissue resurfacing, Journal of Biomedical Materials Research, 39 (1998) 266-276.

[28] Tan,W., Desai,T.A., Microfluidic patterning of cellular biopolymer matrices for biomimetic 3-D structures, Biomedical Microdevices, 5 (2003) 235-244.

CHAPTER 6

CONCLUSION

6.1 Summary

In this dissertation, we have demonstrated two wholly different methods of controlling the nanoscale placement of proteins. This capability is an enabling technology for a wide variety of applications in biotechnology, biological research, and integrated bioMEMS. In the process of pursuing this goal, we have also contributed to the growing body of observed sub-threshold optically induced damage, hopefully lending some insight into the interactions of ultrafast laser irradiation and glass and biological media.

Our demonstration of protein patterning via nano-imprint lithography in Chapter 2 provides a high-throughput and low-cost method to pattern proteins with nanoscale resolution and high specificity. The method is relatively straight-forward and compatible with both conventional substrates used in MEMS fabrication (e.g. silicon), and optical grade glass, making the technique valuable both to bioMEMS and biotechnological devices and development of basic research tools.

In Chapter 3, we demonstrated selective removal of proteins from glass surfaces with nanoscale precision and resolution using tightly focused ultrafast laser irradiation. In doing so, we have established some basic parameters for this technique. We have established the threshold fluence necessary for protein removal to be approximately 1J/cm2 and correlated the size of the removal region as a function of incident fluence, finding an effective minimum feature size on the order of 100nm. This threshold fluence is significantly below the ablation threshold for glass or water, enabling protein to be removed without catastrophically damaging the underlying substrate.

Notably, we see evidence of removal or damage to immobilized biomolecules resulting from single pulses at fluences considerably below the optical breakdown threshold for water. To date, sub-threshold damage to biological structures has primarily been observed only after many pulses have interacted with the sample. Though one may fairly presume that the individual sub-threshold pulses generate damage in such cases, damage resulting from individual sub-threshold pulses has not before, to our knowledge, been compellingly demonstrated.

We have also demonstrated, in Chapter 4, that glass surfaces exposed to ultrafast radiation adopt a long-lived change in surface chemistry, significantly altering their surface charge and thus the propensity of proteins to adsorb to the surface. By examining the adsorption of charged fluorophore molecules, we

have estimated the glass surface charge to be linearly dependent on the incident fluence. Though the nature of and mechanism behind this change in surface chemistry is not entirely clear, we expect that it is predominantly the result of dehydroxylation of silanol groups on the silica surface caused primarily by multiphoton absorption which causes the hydroxyl group of the silanol to dissociate.

We also observed that proteins are immobilized on the glass surface before irradiation, subsequent protein adsorption is significantly affected. From this, we infer that, although AFM and epi-fluorescent assays described in Chapter 3 seemed to show complete protein removal from irradiated areas, there is in fact a residue of some sort that remains after proteins are apparently removed by irradiation. The nature of this residue is unclear. It could potentially be denatured protein, protein fragments, or even covalent functionalization of the glass surface.

Finally, we demonstrated one possible application of in situ protein removal by guiding cell motility through selective removal of the extracellular matrix protein fibronectin near motile fibroblasts. This rather simple application demonstrates a broader capability of this technique, enabling modification of the micro- and nano-scale environment around cells during observation. This may facilitate study of cellular response to patterned biomolecules. Generally, to do so, one must pattern a substrate with a pre-defined pattern and then seed cells, hoping

that a cell exhibiting a desired behavior will interact with your pattern in the desired orientation. Our technique, however, allows one to instead simply find any cell exhibiting the characteristics of import for your study, and then generate an arbitrary pattern near that cell.

6.2 Future Work

In Chapter 3, we have demonstrated the apparent removal of proteins from a glass surface using ultrafast laser irradiation with nanoscale resolution. The exact mechanism behind this removal, however, is unclear. Probing the mechanisms responsible for this removal not only aids in understanding the process of laser removal of proteins, but aids in a broader understanding of the interaction between light, particularly intense pulses of very short duration, and biological media. The likely effects of this interaction may be categorized as thermal, chemical, and acoustic. The relative contribution of these effects remains to be clarified.

One may propose that an increase in temperature in the focal region might cause proteins to denature. Given the small amount of total energy and the small focal volume, though, any increase in temperature will be very short-lived. Even if a protein's environment exceeds a temperature at which denaturation would normally be expected (e.g. 100C), it is not immediately clear whether this transient increase in temperature, will have any effect due to the extremely short

time spent at that temperature. In describing the mechanism of laser-based protein removal, the it will be important to ascertain the contribution of thermal effects such as this.

If the mechanism behind the protein removal or damage is chemical in nature, is it a product of free electrons generated by ionization of water molecules, downstream ROS resulting from interaction of water with those electrons, or direct photochemical interaction with the glass surface or immobilized proteins. All these mechanisms are plausible, and it is possible that they all contribute to some degree.

To begin to tease out what effects are important, one may examine the order of the dependence of the damage or removal effect on the intensity of the incident laser irradiation. For example, the experiment described in Section 3.4 may be performed using pulses of a significantly shorter wavelength. This will allow more sensitive probing of the order of various processes purported to be involved in the damage. For example, a shorter wavelength around 280nm will generate damage in the proteins themselves in a first order process. Excitation of free electrons in the water, however, will remain a two-photon process.

A second perturbation we would recommend is a shortening of the pulse duration. Reducing the pulse duration reduces the total energy deposited in the focal volume, and thereby reducing the effects of thermal and acoustic damage

pathways. In this way, the chemical damage, due to either direct excitation of electrons in the protein or generation of reactive radicals from the bulk water.

The bending of microtubules observed in section 3.3 indicates that there is a significant acoustic shock wave generated at the fluences where we see protein removal. A systematic look at this bending may provide a means of estimating the magnitude of this acoustic effect.

In Chapter 4, we observed that the adsorptive behavior of a target protein on an irradiated glass surface differs depending on whether the surface was uncoated or previously coated with protein prior to irradiation. This result indicates that the initially adsorbed protein is not totally and cleanly removed, and that instead there is some residue or surface modification resulting from the initial protein adsorption. This residual effect could simply be protein which has denatured, flattening on the surface sufficiently so as to appear relatively smooth under AFM. These denatured proteins would be expected to affect subsequent protein adsorption on the surface.

We also inferred in section 3.4 that the inter-raster spacing necessary to totally remove protein from a region is significantly smaller than that presumed by measuring the ablation line width using AFM. It is also possible that, in our observations of adsorption on irradiated surfaces which had been previously coated, that the inter-raster spacing was insufficient to completely remove protein

from the entire region, and the residual protein remaining in the interstices between laser damage spots affect subsequent protein adsorption.

There is also a more speculative possibility that the glass surface has been directly functionalized. Proteins have a number of potentially reactive functional groups which could conceivably covalently bind to the silica surface with sufficient energy input. This energy could potentially be instantiated by direct photochemical bond rearrangement or indirectly through the action of energized electrons from the solution. If this laser-enabled surface modification is observed, it may enable quick functionalization of glass surfaces under low-temperature conditions.

We have interpreted the results of protein and charged fluorophore adsorption to irradiated glass in Sections 4.2 and 4.3 to indicate that irradiation of the glass surface alters the glass surface charge by altering the density of silanol groups on the surface. This interpretation warrants further attention. We performed preliminary studies of the silica surface before and after irradiation using fourier-transform infrared spectroscopy (FTIR), in which the constituent chemical bonds of a sample are inferred based on their characteristic spectrum of absorption of incident infrared light. This technique has been used successfully to characterize the relative portion of silanol and siloxane groups on silica<ref>. However, our efforts were confounded by the small surface areas irradiated coupled with the low reflectivity of the silica surface, which led to a low S/N ratio, and the fact that

silanol surface density is heavily influenced by the degree of hydration of the surface. Though the spectra we obtained were qualitatively consistent with the expected spectrum of a silica surface, we were unable to quantify the silanol surface density due to these two factors. We believe that obtaining these spectra under vacuum, or at least dehydrated, conditions may lead to better results. It should be possible using FTIR to evaluate not only the surface density of silanol groups, but also identify organic bonds characteristic of biomolecules (e.g. C-N, C-C, or C-O), or bonds associated with the speculated covalent modification of the silica surface mentioned above (e.g. Si-N, Si-C).

In addition to examining the underlying mechanisms behind the results we have presented, considerable work remains in characterizing and optimizing the techniques remains to be done. For example, how long do the purported changes in surface chemistry exist? How is protein removal or surface modification affected by buffer conditions such as ionic strength and pH? How is glass surface charge affected when irradiated in air rather than under aqueous buffer?

Beyond elucidating the mechanism behind the techniques we have demonstrated, these techniques are really just tools, and the most interesting future work is in the application of these tools. We have mentioned elsewhere, in Chapters 1 and 5, a sampling of the myriad cellular studies which protein

patterning enables, helping to lend insight into a variety of basic biological mechanisms.

6.3 Concluding Remarks

The work presented in this work signifies a significant contribution to the field of protein patterning. We hope that the techniques such as those detailed here, enhancing capabilities in the placement of proteins with ultra-high resolution, down to the scale of individual proteins, will provide tools to biologists and biotechnologists that allow them to advance the next generations of biosensor, bioMEMS, and biological assays. These ultra-high resolution techniques hold promise not only to incrementally improve performance characteristics of biosensors, such as quickening assay speed, reducing required reactant volumes, or expanding the number of assays performed in a single test; but these methods also hold potential to enable new capabilities in devices and assays. With these techniques, we may exploit biomolecules to perform useful work in microdevices, integrate biological functionality into so-called lab-on-a-chip microanalysis systems, and we can study biological phenomena which are difficult to probe with existing techniques, such as spatial regulation of cellular behavior. We believe that these, and other, diverse, exciting, and important fields in biotechnology and biological research can benefit from the protein patterning work detailed here.